REPORT DOCUMENTATION PAGE

Form Approved
OMB No. 0704-0188

1. AGENCY USE ONLY *(Leave blank)*	2. REPORT DATE	3. REPORT TYPE AND DATES COVERED
	November 16, 1998	Technical Report # 42

4. TITLE AND SUBTITLE
Probing Structure-Property Relationships in Third-Order Nonlinear Optical Polymers: Third Harmonic Generation Spectroscopy and Theoretical Modeling of Systematically Derivatized Conjugated Aromatic Polyimines.

5. FUNDING NUMBERS
N00014-94-1-0540
Kenneth J. Wynne
R & T Code 3132111

6. AUTHOR(S)
Chen-Jen Yang, Samson A. Jenekhe, Jeffrey S. Meth and Herman Vanherzeele

7. PERFORMING ORGANIZATION NAMES(S) AND ADDRESS(ES)
University of Rochester
Department of Chemical Engineering
206 Gavett Hall, Box 270166
Rochester. NY 14627-0166

8. PERFORMING ORGANIZATION REPORT NUMBER
42

9. SPONSORING / MONITORING AGENCY NAMES(S) AND ADDRESS(ES)
Office of Naval Research
800 North Quincy Street
Arlington, VA 22217-5000

10. SPONSORING / MONITORING AGENCY REPORT NUMBER

11. SUPPLEMENTARY NOTES
Ind. Eng. Chem. Res., in press.

a. DISTRIBUTION / AVAILABILITY STATEMENT
Reproduction in whole or in part is permitted for any purpose of the United States Government. This document has been approved for public release and sale; its distribution is unlimited.

12. DISTRIBUTION CODE

13. ABSTRACT *(Maximum 200 words)* Picosecond third harmonic generation (THG) spectroscopy in the range 0.9-2.4 μm (0.52-1.38 eV) combined with sum-over-states (SOS) theoretical modeling have been used to investigate the third-order nonlinear optical properties of a series of 9 conjugated aromatic polyimines designed to elucidate structure-$\chi^{(3)}$ relationships in conjugated polymers. The THG-measured frequency dispersed third-order susceptibility $\chi^{(3)}$ of the series of polymers has off-resonant and three-photon resonance-enhanced values in the range of 1.1×10^{-12} to 2.0×10^{-11} esu and 6.4×10^{-12} to 7.2×10^{-11}esu, respectively, demonstrating a large modulation of nonlinear optical response by simple structural variations. A random copolymer was found to have enhanced $\chi^{(3)}$ compared to either of its parent homopolymers. Asymmetric donor side-group substitutions was found to result in 7-10-fold enhancement of off-resonant $\chi^{(3)}$ compared to either symmetric substitutions or no substitutions. Theoretical three- and four-level SOS models, justified by site-selective fluorescence spectroscopy, were found to describe the $\chi^{(3)}$ dispersion data and the observed multiphoton resonances very well. The zero-frequency $\chi^{(3)}$ was predicted from the SOS models to be negative for eight of the nine polymers and to be in the range of -0.43 to -8.12×10^{-12} esu, the magnitudes of which are very close to observed off-resonance values at 2.4 μm (0.52 eV). Negative real part of $\chi^{(3)}(-\omega;\omega,-\omega,\omega)$ over a wide wavelength range of ($\lambda>1.38$ μm) was also predicted by the SOS Models for the same eight polymers with strong one-photon and two-photon resonances, suggesting that they would exhibit self-defocusing phenomena. Similarly predicted $\chi^{(3)}(-\omega;\omega,-\omega,\omega)$ spectra of the polyimines suggest that third-order susceptibility measured by degenerate four wave mixing would be up to two orders of magnitude larger than values measured by THG spectroscopy.

14. SUBJECT TERMS
Nonlinear optical polymers; third harmonic generation spectroscopy; theoretical modeling; conjugated polymers; aromatic polyimines; aromatic polyazomethines; degenerate four-wave mixing.

15. NUMBER OF PAGES
63

16. PRICE CODE

17. SECURITY CLASSIFICATION OF REPORT	18. SECURITY CLASSIFICATION OF THIS PAGE	19. SECURITY CLASSIFICATION OF ABSTRACT	20. LIMITATION OF ABSTRACT
Unclassified	Unclassified	Unclassified	Unlimited

OFFICE OF NAVAL RESEARCH

GRANT NO: N00014-94-1-0540

R&T Code 3132111
Kenneth J. Wynne

Technical Report NO. 42

Probing Structure-Property Relationships in Third-Order Nonlinear Optical Polymers: Third Harmonic Generation Spectroscopy and Theoretical Modeling of Systematically Derivatized Conjugated Aromatic Polimines

By

Chen-Jen Yang, Samson A. Jenekhe, Jeffrey S. Meth and Herman Vanherzeele

Prepared for Publication

In

Ind. Eng. Chem. Res., in press.

Department of Chemical Engineering
and Center for Photoinduced Charge Transfer
University of Rochester, New York 14627

February 4, 1998

Probing Structure-Property Relationships in Third-Order Nonlinear Optical Polymers: Third Harmonic Generation Spectroscopy and Theoretical Modeling of Systematically Derivatized Conjugated Aromatic Polyimines.

Chen-Jen Yang and Samson A. Jenekhe*

Departments of Chemical Engineering and Chemistry and Center for Photoinduced Charge Transfer, University of Rochester, Rochester New York 14627-0166

Jeffrey S. Meth and Herman Vanherzeele

DuPont Central Research and Development Department, Wilmington, Delaware 19880-0356

Abstract. Picosecond third harmonic generation (THG) spectroscopy in the range 0.9-2.4 μm (0.52-1.38 eV) combined with sum-over-states (SOS) theoretical modeling have been used to investigate the third-order nonlinear optical properties of a series of 9 conjugated aromatic polyimines designed to elucidate structure-$\chi^{(3)}$ relationships in conjugated polymers. The THG-measured frequency dispersed third-order susceptibility $\chi^{(3)}$ of the series of polymers has off-resonant and three-photon resonance-enhanced values in the range of $1.1x10^{-12}$ to $2.0x10^{-11}$ esu and $6.4x10^{-12}$ to $7.2x10^{-11}$esu, respectively, demonstrating a large modulation of nonlinear optical response by simple structural variations. A random copolymer was found to have enhanced $\chi^{(3)}$ compared to either of its parent homopolymers. Asymmetric donor side-group substitutions was found to result in 7-10-fold enhancement of off-resonant $\chi^{(3)}$ compared to either symmetric substitutions or no substitutions. Theoretical three- and four-level SOS models, justified by site-selective fluorescence spectroscopy, were found to describe the $\chi^{(3)}$ dispersion data and the observed multiphoton resonances very well. The zero-frequency $\chi^{(3)}$ was predicted from the SOS models to be negative for eight of the nine polymers and to be in the range of –0.43 to $-8.12x10^{-12}$ esu, the magnitudes of which are very close to observed off-resonance values at 2.4 μm (0.52 eV). Negative real part of $\chi^{(3)}(-\omega;\omega,-\omega,\omega)$ over a wide wavelength range of (λ> 1.38 μm) was also predicted by the SOS Models for the same eight polymers with strong one-photon and two-photon resonances, suggesting that they would exhibit self-defocusing phenomena. Similarly predicted $\chi^{(3)}(-\omega;\omega,-\omega,\omega)$ spectra of the polyimines suggest that third-order susceptibility measured by degenerate four wave mixing would be up to two orders of magnitude larger than values measured by THG spectroscopy.

* To whom correspondence should be addressed.

Introduction

Materials that combine large third-order optical nonlinearity with optical transparency are necessary for a range of photonic device applications such as all-optical switches, optical signal processing, sensor protection, and optical phase conjugation.[1-21] Since the pioneering work of Sauteret et al.,[1c] which showed that the polydiacetylenes exhibit large third-order optical nonlinearities with ultrafast response times, π-conjugated polymers have been central to the search for third-order nonlinear optical materials. The third-order nonlinear optical properties of numerous conjugated polymers have thus been investigated, including: polydiacetylenes,[1c, 13, 14] polyacetylene,[12] polythiophenes,[10a, 15, 16] polyanilines,[21a, 22] poly(p-phenylene vinylenes),[17] polyquinolines,[22a] polyimines (aromatic Schiff base polymers),[21c] and poly(p-phenylene benzobisazoles).[23] Reviews of the extensive experimental and theoretical studies of the third-order nonlinear optical (NLO) properties of conjugated polymers have been published.[3, 5] Although π-conjugated polymers have the largest *nonresonant* third-order NLO susceptibility ($\chi^{(3)}$) with ultrafast response times (<1 ps) among all classes of materials, the measured off-resonant $\chi^{(3)}$ values in the range of 10^{-12} to 10^{-9} esu are still orders of magnitude less than the projected requirements for practical photonic applications.[1, 6] Understanding of the structure-property relationships that underlie the third-order NLO properties of conjugated molecules and polymers is currently lacking but is required to guide the rational design of polymers with enhanced optical nonlinearities and optical transparency.[8, 21-23]

Although $\chi^{(3)}$ data have been reported for numerous conjugated polymers in the past 20 years, reliable quantitative comparison between the same or different polymers and inference of structure-$\chi^{(3)}$ correlations from such data are not currently feasible. The main reasons for this include the tensorial (4th rank) nature of the third-order NLO susceptibility and its frequency

dispersion.[3e, 4, 24] Different techniques such as third harmonic generation (THG) and degenerate four wave mixing (DFWM) have been used to measure different components of $\chi^{(3)}$ at different wavelengths, e.g. $\chi^{(3)}$ $(-3\omega;\omega,\omega,\omega)$ by THG and $\chi^{(3)}$ $(-\omega;\omega,-\omega,\omega)$ by DFWM.[3e, 3g, 4] Also, until recently most $\chi^{(3)}$ data were available at only one or a few wavelengths, which may not be away from multiphoton resonances of the polymers. Knowledge of the frequency dispersion of $\chi^{(3)}$ over a sufficiently wide spectral range that enables the off-resonant and the multiphoton resonance-enhanced $\chi^{(3)}$ values to be distinguished unambiguously is essential to probing the structure-$\chi^{(3)}$ relationships of polymers.[10, 12a, 17c, 21-25]

The second hyperpolarizability (γ) of conjugated molecules and oligomers has been investigated extensively by both theoretical and experimental techniques for the purpose of elucidating structures- γ relationships.[8, 9, 26-32] For example, theoretical and experimental studies of polyenes and oligothiophenes have confirmed the scaling law $\gamma \sim L_d^k \sim N^k$, where L_d is conjugation length and N is chain length or number of π electrons of the conjugated molecule. The power law exponent k has variously been predicted or measured to be in the range 3-8 for different conjugated molecules or oligomers.[9, 26-30, 31a] Such structure-γ correlations have frequently been assumed to extend to conjugated polymers. Although theoretical and experimental studies of structure- γ relationships in conjugated small molecules and oligomers can shed some light on the structure- γ and structure-$\chi^{(3)}$ properties of conjugated polymers, there are important structural features of polymers that could be completely missed in oligomers. Among these possible differences between conjugated oligomers and polymers are the followings. (1) It is well known that the excited state electronic structure of a conjugated polymer can be qualitatively and quantitatively different from that of its oligomer;[29] the relative ordering of the nB_u and mA_g excited states can be different as for example the $1B_u$ excited state

being lower lying than the $2A_g$ excited state in oligomers whereas the $2A_g$ is lower lying than the $1B_u$ in the corresponding polymer.[11] (2) The conformation and geometry of a polymer can be very different from those of its oligomers just as are the effects of side-group substituents.[33] (3) There are no ways of simulating certain features of a polymer chain structure in an oligomer, e.g. random or block copolymerization.[34] The failure of oligomer-derived structure -$\chi^{(3)}$ relationships when applied to the corresponding polymers have been previously reported.[23,32]

Our approach to the problem of elucidating the structure- $\chi^{(3)}$ relationships of conjugated polymers consists of (1) synthesis, structural characterization and processing into thin films of a series of systematically designed polymers within a structural class,[35,36] (2) measurement of the $\chi^{(3)}$ $(-3\omega;\omega,\omega,\omega)$ spectra for the series of related polymers, (3) use of sum-over-states (SOS) theoretical models based on the time-dependent perturbation theory to analyze the $\chi^{(3)}$ spectra, and (4) correlation of the off-resonant, multiphoton resonant, or other aspects of the $\chi^{(3)}$ spectra data to the molecular and electronic structures of the polymers. Efficacy of this approach rests in part on the fact that the SOS theory relates the frequency dispersed third-order optical response of a material to its ground and excited state electronic structures as characterized by the energy levels and the transition dipole moments connecting them. Thus, knowledge of the excited-state and ground-state energy levels and their associated transition dipole moments can provide information about the frequency dispersed $\chi^{(3)}$ and vice versa. It is this ability of the SOS theory to simulate the $\chi^{(3)}$ spectra of materials in terms of their as yet unknown energy levels and transition dipole moments that we exploit for correlating observed $\chi^{(3)}$ to the molecular and electronic structures of *related* polymers. In this way the structural origins of observed $\chi^{(3)}$ variations can be isolated and structure- $\chi^{(3)}$ functions applicable to polymers extracted. We have previously applied such an approach to a number of different classes of conjugated polymers,

including: polyquinolines,[22a] polyanilines,[21a, 22b] polybenzobisazoles,[23, 37] and polybenzimidazolebenzophenanthrolines.[38]

In this paper, we report the $\chi^{(3)}$ spectra obtained by picosecond third harmonic generation spectroscopy in the wavelength range 0.9-2.4 μm (0.52-1.38 eV) for a series of 9 derivatized conjugated aromatic polyimines (Schiff base polymers) whose molecular structures are shown in chart 1. The parent conjugated polyimine, poly(1,4-phenylenenitrilomethylidyne-1,4-phenylene methylidynenitrilo) (**1a**, PPI), is systematically derivatized through backbone variation (**4a, 4b, 4c,**), side-group substitutions (**1b, 3a, 3b, 3c**), and random copolymerization (**2a**). These simple variations in the molecular structure of the aromatic polyimines can be expected to result in a large modulation of the electronic ground state and excited state structures and corresponding modulation of the nonlinear optical properties of this class of conjugated polymers. Thus, the approach to probing structure -$\chi^{(3)}$ relationships described in the previous paragraph is applied here to the *polyimines* (or polyazomethines). Applicability of the three- and four-level SOS theoretical models to describing the third order NLO response of the polyimines was confirmed both by site-selective photoluminescence spectroscopic characterization of the materials and the theoretical analysis of the $\chi^{(3)}$ dispersion data. Some of the specific structural effects on $\chi^{(3)}$ explored include: electronic delocalization as characterized by the lowest energy π-π^* optical transition; size of polymer repeat unit; symmetric and asymmetric electron donating side-group substitutions; random copolymer structure which destroys translational symmetry or periodicity; and intramolecular charge transfer/excited state proton transfer. A preliminary communication has previously reported the experimental $\chi^{(3)}$ data for two of the polyimines (**1a, 3a**) but not the SOS theoretical model analysis.[21c]

Experimental Section

Synthesis and Characterization of Polymers. All the polymers in chart 1 were prepared by the solution condensation polymerization of aromatic diamines and aromatic dialdehydes in hexamethylenephosphoramide (HMPA)/1-methyl-2-pyrrolidone(NMP) solvent.[36, 39] Addition of LiCl to the polymerization medium, to absorb the water by product, ensured achievement of high molecular weight, and good film-forming polymers. The detail synthesis and characterization of the polymers is reported elsewhere.[36] Characterization of the molecular and electronic structures of the polymers was done by ^{1}H NMR and FTIR spectroscopies, thermogravimetric analysis (TGA), differential scanning calorimetry (DSC), UV-visible absorption spectroscopy, photoluminescence spectroscopy, and cyclic voltammerty.[36]

Preparation of Thin Films. The processing of aromatic polyimines into excellent optical quality thin films was through spin coating of soluble Lewis acid ($GaCl_3$ or $AlCl_3$) coordination complexes of the polymers.[35, 36] The reversibility of the complexation-decomplexation processes, which ensured thin films of the pure polymers, was verified by TGA, FTIR, UV-Vis, and electrochemical experiments.[36] The thin films were amorphous as judged by their optical transparency and excellent uniformity.

Measurement of Refractive Index. The wavelength-dependent refractive indices of the polymers were deduced from the interference fringes in their optical transmission spectra as described by Manafacier et al.[40] and Swanepoel.[41] The refractive index n is given by

$$n(\lambda) = \frac{m\lambda}{2d} \qquad (1)$$

where λ is wavelength, d is film thickness, and m is order number deduced from the transmission spectrum by a linear-regression computer program. The film thickness d was independently

measured by using a profilometer. Our prior use of this technique for the determination of the refractive indices of various conjugated polymers has been reported. [42]

Absorption and Fluorescence Spectra. Optical absorption spectra of polymer thin films were obtained by using a Perkin-Elmer Model Lambda 9 UV-Vis- near IR spectrophotometer. Steady-state photoluminescence (PL) spectra of thin films were obtained on a Spex Fluorolog-2 fluorimeter equipped with a Spex DM3000F spectroscopy computer. The polymer films on glass slides were positioned such that the emission was detected at 22.5° from the incident beam. All the photophysical measurements were done at room temperature as previously described. [34]

Measurement of $\chi^{(3)}$ Spectra. Third harmonic generation (THG) experiments were performed on a picosecond system based on a mode-locked Nd:YLF laser. This versatile laser system, which has been described in full detail elsewhere, [37,43] operates in two modes: CW(100 MHz) and pulse (10 Hz). The tuning range is 0.6 μm~4.0 μm. The pulse duration can also be selected independently of the other operating parameters: either short(typically 5 ps) or long(typically 50 ps) pulses are available. In this work, we used the output of the parametric generation/amplifier consisting of a pair of single 35-45 ps pulses (signal and idler) with energy> 0.5 mJ each anywhere in the tuning range. Pulse-to-pulse energy fluctuations do not exceed 5%.

During the THG experiment, the sample(fused silica as the reference materials and/or the polymer film under study on a silica substrate) is located in a vacuum cell to remove undesirable contributions from air to the THG signal from the sample. The sample is rotated about a vertical axis to generate a THG Maker fringe pattern. In the reference path a (stationary) highly nonlinear polymer film on a silica substrate is used to generate the third harmonic. The thickness of this film is chosen to be smaller than the coherence length to avoid Marker fringes in the THG signal, yet it is thick enough to give a THG signal that is two or more orders of magnitude larger

than that from the substrate (to avoid interference). To improve the signal to noise ratio (S/N), all laser shots are rejected for which either the energy of the fundamental or the third harmonic in the reference arm fall outside predetermined windows. In this way instabilities (both in energy per pulse and pulse width) of the laser source are effectively reduced to 1%. By taking the ratio of the THG signals in both arms, the effect of fluctuation in both power and pulse width of the fundamental beam are further eliminated. Finally, averaging this ratio of some 250 laser shots yields a precision of typically ±0.5%.

The magnitude of the third-order susceptibility $\chi^{(3)}$ $(-3\omega;\omega,\omega,\omega)$ of the sample (thin polymer film on a fused silica substrate) is obtained relative to fused silica by comparing the Maker fringe patterns of the sample and fused silica.[37,38] The resulting approximate $\chi^{(3)}$ value is then used as a starting value for the exact fitting procedure.[44,45] However, the large optical nonlinearity of the polymer films studied in this work made the use of the exact fitting technique impractical for some samples. Therefore, only the magnitude and not the phase of $\chi^{(3)}$ $(-3\omega;\omega,\omega,\omega)$ is reported here. For the silica substrate, we used a value of $\chi^{(3)}=2.8 \times 10^{-14}$ esu at 1.9 μm.[46] In order to correct this value for dispersion, we used Miller's rule as a simple approximation.[37]

Theoretical Models

The time-dependent perturbation theory has been widely used as a basic starting point to describe the optical nonlinearities of organic materials.[37, 47-52] This theory, which is used in the present work to interpret the experimental $\chi^{(3)}$ dispersion data, starts with the full perturbation expression for the second hyperpolarizability of a molecular system involving a sum over all excited states of the system. This expression for the second hyperpolarizability, $\gamma(-3\omega;\omega,\omega,\omega)$, including homogeneous broadening is [37,47]

$$\gamma(-3\omega;\omega,\omega,\omega) = \frac{e^4}{4\,\hbar^3} \sum_{l,m,n} \left\{ \frac{\langle g|p|l\rangle \langle l|p|m\rangle \langle m|p|n\rangle \langle n|p|g\rangle}{(\omega_{gl}-3\omega-i\Gamma_{gl})(\omega_{gm}-2\omega-i\Gamma_{gm})(\omega_{gn}-\omega-i\Gamma_{gn})} + \right.$$

$$\frac{\langle g|p|l\rangle \langle l|p|m\rangle \langle m|p|n\rangle \langle n|p|g\rangle}{(\omega_{gl}+\omega+i\Gamma_{gl})(\omega_{gm}-2\omega-i\Gamma_{gm})(\omega_{gn}-\omega-i\Gamma_{gn})} + \frac{\langle g|p|l\rangle \langle l|p|m\rangle \langle m|p|n\rangle \langle n|p|g\rangle}{(\omega_{gl}+\omega+i\Gamma_{gl})(\omega_{gm}+2\omega+i\omega_{gm})(\omega_{gn}-\omega-i\Gamma_{gn})}$$

$$\left. + \frac{\langle g|p|l\rangle \langle l|p|m\rangle \langle m|p|n\rangle \langle n|p|g\rangle}{(\omega_{gl}+\omega+i\Gamma_{gl})(\omega_{gm}+2\omega+i\Gamma_{gm})(\omega_{gn}+3\omega+i\Gamma_{gn})} \right\} - \frac{e^4}{4\,\hbar^3} \sum_{l,n} \left\{ \frac{\langle g|p|l\rangle \langle l|p|g\rangle \langle g|p|n\rangle \langle n|p|g\rangle}{(\omega_{gl}-3\omega-i\Gamma_{gl})(\omega_{gl}-\omega-i\Gamma_{gl})(\omega_{gn}-\omega-i\Gamma_{gn})} \right.$$

$$+ \frac{\langle g|p|l\rangle \langle l|p|g\rangle \langle g|p|n\rangle \langle n|p|g\rangle}{(\omega_{gl}-\omega-i\Gamma_{gl})(\omega_{gn}+\omega+i\Gamma_{gn})(\omega_{gn}-\omega-i\Gamma_{gn})} + \frac{\langle g|p|l\rangle \langle l|p|g\rangle \langle g|p|n\rangle \langle n|p|g\rangle}{(\omega_{gl}+3\omega+i\Gamma_{gl})(\omega_{gl}+\omega+i\Gamma_{gl})(\omega_{gn}+\omega+i\Gamma_{gn})}$$

$$\left. + \frac{\langle g|p|l\rangle \langle l|p|g\rangle \langle g|p|n\rangle \langle n|p|g\rangle}{(\omega_{gl}+\omega+i\Gamma_{gl})(\omega_{gn}-\omega-i\Gamma_{gn})(\omega_{gn}+\omega+i\Gamma_{gn})} \right\} . \qquad (2)$$

In which g represents the ground state, 1, m, and n represents excited states of the system; ω_{gl} and Γ_{gl} and the like represent the transition frequencies and the damping coefficients, respectively. The matrix elements are the transition dipole moments between states. The dummy variables 1, m, and n include all states except the ground state. Intuitively, one sees that because there exists an infinite number of excited states for a polymer molecule it would be very impractical to use the time-dependent perturbation theory of equation (2) to calculate the optical response of polymers. However, recent calculations on finite-length polyenes and other conjugated oligomers have shown that only a small number of states have large transition dipole moments connecting them to each other.[29, 31, 49-51] These states then are the essential states contributing to the nonlinear-optical response of the material and trace out a path in the energy level diagrams as schematically shown in Chart 2. The sum-over-states (SOS) expression of equation (2) greatly simplifies when only a small number of states are considered.

Centrosymmetric conjugated polymers generally have C_{2h} space group from which symmetric (even parity) A_g and antisymmetric (odd parity) B_u states are assigned with respect to the center of inversion.[53,54] According to quantum mechanical optical selection rules, transitions between states of different symmetries such as between A_g and B_u states are allowed, but optical transitions between states of the same symmetry (parity) are not allowed. Consequently, the optical channels contributing to optical nonlinearity (γ) are constructed by recognizing the combination of allowable excitation paths connecting the identified essential A_g and B_u states. The possible optical channels in the triple sum and the double sum of the SOS expression of equation (2) that we use to analyze $\chi^{(3)}(-3\omega;\omega,\omega,\omega)$ spectra are the following.

Two-Level Model. A schematic diagram of a two-level system in which two essential states contribute to NLO response is depicted in Chart 2a. We assign $1A_g$ as the ground state and $1B_u$ as the lowest-lying one-photon excited state. In this case, the optical channel in the SOS two-level model simplifies to:

triple sum = 0

double sum: $1A_g \rightarrow 1B_u \rightarrow 1A_g \rightarrow 1B_u \rightarrow 1A_g$

Since the essential states are the ground state and the lowest lying, transition dipole-allowed, odd-parity excited state, the SOS theory for a two-level model is very similar to band theory in its description of NLO response.[26a]

Three-Level Model. A schematic diagram of the three essential states is shown in Chart 2b. In the three-level model, an A_g excited state, which has a significantly large transition dipole moment connecting it to the 1Bu state, is added compared to the two-level system. As a result, a second pathway, which contributes to the optical nonlinearity with an opposite sign from that of the first one, becomes manifest. It has been suggested that an interference between these two

paths, which may lead to a sharp decrease of the optical nonlinearity at some frequencies can be expected.[37, 38] The optical channels contributing to $\gamma(-3\omega;\omega,\omega,\omega)$ in a three-level SOS model are:

triple sum: $1A_g \rightarrow 1B_u \rightarrow mA_g \rightarrow 1B_u \rightarrow 1A_g$

double sum: $1A_g \rightarrow 1B_u \rightarrow 1A_g \rightarrow 1B_u \rightarrow 1A_g$

Four-Level Model. To obtain a good fit between the SOS theoretical model and experimental $\chi^{(3)}$ dispersion data, especially in the multiphoton-resonance regions, it was found that an additional excited state besides those included in a three-level model is required to describe the third-order optical nonlinearity.[10a, 25, 54] Depending on the parity of this third excited state, two types of four-level models can be constructed. Stegeman et al. have used an nA_g excited state which has a significantly large transition dipole moment connecting it to the $1B_u$ excited state, in addition to an mA_g which is the S_2 state, to fit the $\chi^{(3)}(-3\omega;\omega,\omega,\omega)$ spectra of polydiacetylene, β-carotene, and polythiophene.[25] Mazumdar, Stegeman, and co-workers, however, have used an nB_u excited state, which has a significantly large transition dipole moment connecting it with the mA_g excited state to simulate the same experimental $\chi^{(3)}$ dispersion data.[54] Based on comparisons with the two-photon absorption (TPA) [11] and electroabsorption (EA) spectra of the polymer, it was suggested that the latter approach gives a better physical picture of the third-order NLO response of conjugated polymers. [54] In the present work, we will use the latter four-level model ($1A_g$, $1B_u$, mA_g, nB_u) to analyze our $\chi^{(3)}$ dispersion data. It will be shown subsequently that in some $\chi^{(3)}$ spectra, such as that of MO-PHOPI, there exists three multiphoton-resonance peaks which confirms the inherent requirement of a four-level model to describe the nonlinear optical response of the materials. A schematic diagram of the four-level model is shown in Chart 2c. The optical channels in the four-level model are described as follows:

triple sum: $1A_g \rightarrow 1B_u \rightarrow mA_g \rightarrow 1B_u \rightarrow 1A_g$

$1A_g \rightarrow nB_u \rightarrow mA_g \rightarrow nB_u \rightarrow 1A_g$

$1A_g \rightarrow 1B_u \rightarrow mA_g \rightarrow nB_u \rightarrow 1A_g$

$1A_g \rightarrow nB_u \rightarrow mA_g \rightarrow 1B_u \rightarrow 1A_g$

double sum: $1A_g \rightarrow 1B_u \rightarrow 1A_g \rightarrow 1B_u \rightarrow 1A_g$

$1A_g \rightarrow nB_u \rightarrow 1A_g \rightarrow nB_u \rightarrow 1A_g$

$1A_g \rightarrow 1B_u \rightarrow 1A_g \rightarrow nB_u \rightarrow 1A_g$

$1A_g \rightarrow nB_u \rightarrow 1A_g \rightarrow 1B_u \rightarrow 1A_g$

Our SOS theoretical model analysis of the $\chi^{(3)}$ dispersion data involves the inclusion of a hyperbolic secant function to account for inhomogeneous and vibronic broadening of electronic transitions. This approximation along with the derivation of equation (3) have been described in detail elsewhere.[37, 38] After Kramer-Kronig transformation, equation (3) is obtained as a substitute for the Lorentzian line shape term in the time-dependent SOS equation (2) for the second hyperpolarizability:[37, 38]

$$\frac{1}{\omega_{gl} \pm n\omega \pm i\Gamma_{gl}} \Rightarrow \frac{\pm 1}{iS_{gl}} \sec h\left(\frac{\omega_{gl} \pm n\omega}{S_{gl}}\right) + \frac{\frac{2}{\pi}\left(\omega_{gl} \pm n\omega\right)}{\left(\omega_{gl} \pm n\omega\right)^2 + \left(\frac{\pi S_{gl}}{2}\right)^2} \qquad (3)$$

Equations (2) and (3) coupled with the above optical channels are used to calculate the second hyperpolarizabilty γ for each SOS model. The macroscopic frequency dispersed $\chi^{(3)}$ is

calculated from the second hyperpolarizability by including the Lorentz-Lorenz local field factors according to:

$$\chi^{(3)}(-3\omega;\omega,\omega,\omega) = \frac{N}{5}\left(\frac{n^2(\omega)+2}{3}\right)^3\left(\frac{n^2(3\omega)+2}{3}\right)\gamma(-3\omega;\omega,\omega,\omega) \qquad (4)$$

In this expression the number density N was calculated independently from a theoretical consideration of atomic contributions to the physical density of the materials, [22, 37] and the refractive indices n(ω) and n(3ω) were obtained from the refractive index dispersion data. [42] In particular n(3ω) in the range 300 to 450 nm which was close to the main absorption band was estimated from the Sellmeir equation representation of the n(ω) data.[42] Although the Sellmeir equation was found to reproduce refractive index dispersion data to within ± 1 - 2%, [42] its associated uncertainties and errors in film thickness measurement combine to give errors in the $\chi^{(3)}$ data of ± 10 – 20%. The repeatability of all the $\chi^{(3)}$ data was ± 5%.

Results and Discussion

Optical Absorption Spectra of Polymer Thin Films. Figures 1-3 show the optical absorption spectra of thin films of the conjugated polyimines investigated in this study. The spectrum of PPI **(1a)** in Figure 1 shows that this parent aromatic polyimine absorbs in the visible with a π-π* transition maximum (λ_{max}) at 405 nm and an optical bandgap (E_g) of 2.50 eV as determined from the absorption edge. The optical absorption spectra of PBPI, PSPI, and PBEPI are shown in Figure 1 with that of PPI to reveal the effects of changing the polymer backbone structure on bandgap and λ_{max}. Compared to the absorption spectrum of PPI, the *p*-biphenylene linkage in PBPI results in a negligible change of optical bandgap whereas the Stilbene linkage in PSPI

leads to a bandgap reduction of 0.12 eV. A 0.33 eV increase in optical bandgap is observed in PBEPI as a result of the break of conjugation by the arylene ether linkage compared to PPI, indicating that electron delocalization in this series of polymers extend over two or more repeat units except in PBEPI.

The effects of substitutions on the optical absorption are shown in Figures 2 and 3. In Figure 2, it is seen that the dimethoxy substitution in PMOPI reduces its bandgap to 2.34 eV from 2.50 eV in PPI. A bathochromic shift in the λ_{max} from 405 to 450 nm due to the electron-donating effect of dimethoxy group is clearly evident. There is also an increase of the absorption coefficient (hyperchromic shift) in PMOPI compared to PPI. A similar dihydroxy substitution significantly reduces the bandgap from 2.50 to 2.07 eV and the corresponding λ_{max} is shifted to about 495 nm in PHOPI. Since the OH group has slightly lower electron-donating ability than the OCH_3 group, the much larger bathochromic shift in the dihydroxy-substituted polymer (PHOPI) compared to its dimethoxy-substituted counterpart (PMOPI) suggests that intramolecular hydrogen bonding, which was verified by comparing the FTIR spectra of the polymer and its $CaCl_3$ complex,[36a] has a dramatic effect on the electronic structure other than the inductive effect of the hydroxy group. Also shown in Figure 2 is the optical absorption spectrum of MO-PHOPI (**3c**) which shows that a further modification of molecular structure by substitution on PHOPI results in only a small further reduction of bandgap in MO-PHOPI (E_g=2.03 eV) compared to PHOPI. The optical absorption spectra of PPI, PMPI, and the copolymer PPI/PMPI in Figure 3 reveal that methyl substitution in PMPI and random copolymerization as in PPI/PMPI (53 mol % PPI) do not alter the λ_{max} and E_g values compared to PPI.

The observed large bathochromic shift of the absorption spectrum of PHOPI compared to both PPI and PMOPI can be understood in terms of intramolecular hydrogen bonding-induced conformation change, which facilitates a more coplanar structure compared to either PPI or PMOPI. It is well known from the X-ray crystal structure of *trans*-N-benzylideneaniline, a model compound of PPI, that the N-phenyl ring is twisted 55° from the plane of the imine group (CH=N) due to the conjugation between the nitrogen lone pair electrons and the π-electrons on the adjacent benzene ring. [55,56] Our prior studies of $GaCl_3$ and diarylphosphate complexes of conjugated polyimines showed that complexation resulted in a large bathochromic shift of the absorption spectrum relative to that of the parent polymer.[36,57] The net effect of either hydrogen bonding to the imine nitrogens of PHOPI and MO-PHOPI or their complexation by Lewis acids or protonic acids is a more coplanar molecular structure which is favorable to greater electronic delocalization in the ground state. Although there is a small bathochromic shift in going from PHOPI to MO-PHOPI, it is the intramolecular hydrogen bonding in both polymers that dominates their ground-state electronic structures.

The λ_{max} of the lowest energy π-π* transition and optical bandgap E_g determined from the absorption edge are listed in Table 1. These absorption data reflect the extent of electron delocalization and the ground state electronic structure of the series of polyimines in chart 1. As shown in Table 1, the smallest bandgaps in these polymers are achieved in the two dihydroxy derivatives (PHOPI, MO-PHOPI). The wide range of ground state electronic structure variation and the associated broad bandgap range (2.03-2.83 eV) offer an opportunity to investigate the effects of structure on the third-order nonlinear optical properties of polymers. One interesting questions is whether or not the $\chi^{(3)}$ will scale as $1/E_g^k$ as long predicted (k=6) from band theory,[26] and commonly observed in some conjugated oligomers. [28,32,58]

Refractive Index Dispersion. Information on the wavelength dispersion of the refractive index of the polymers is required to determine the local field correction factors and obtain $\chi^{(3)}$ from γ according to equation (4). The wavelength dispersed refractive index data obtained according to equation (1) were fit into a three-term Sellmeir equation as a means of achieving facile and accurate interpolation between measured values. The Sellmeir dispersion expression for refractive index is well known to accurately describe the wavelength dependent refractive indices of inorganic glass and non-glass materials as well as those of organic molecules and polymers.[59-60]

Figure 4 shows the optical transmission spectrum of PMPI along with the refractive index dispersion data measured therefrom. The solid line through the data points in Figure 4 is the following three-term Sellmeir equation:

$$n^2 = 1+\frac{0.0276\lambda^2}{\lambda^2 - 0.2586^2}+\frac{0.0690\lambda^2}{\lambda^2 - 0.2581^2}+\frac{1.6511\lambda^2}{\lambda^2 - 0.2625^2} \qquad (5)$$

The wavelength λ in equation (5) is in units of μm. The Sellmeir equation describes the refractive index dispersion of PMPI very well as seen in Figure 4. Similar data and their Sellmeir equation fit were obtained for the remaining polymers and used in the calculation of $\chi^{(3)}$ according to equation (4). Because such wavelength dispersed refractive index data are useful for other purposes they are collected together with those of other conjugated polyimines and discussed in detail elsewhere.[42]

Site-Selective Fluorescence Spectroscopy and Nature of the Excited States of Conjugated Polyimines. How best to describe the excited states of π-conjugated polymers has been the subject of considerable debate.[61-63] The view that conjugated polymers are one-dimensional

semiconductors which exhibit band-to band optical transitions has been very influential in the theoretical and experimental studies of third-order NLO properties in conjugated polymers.[26-28, 61] More recently, however, an alternative view that the excited states of conjugated polymers are molecular excitons in nature has received both theoretical and experimental support.[30, 62, 63] Mukamel and co-workers have developed an elegant theory of the optical and nonlinear optical properties of conjugated polymers in which molecular excitons are the fundamental excited states. [30] This excitonic theory has been used successfully to reproduce the $\chi^{(3)}$ spectra of polyacetylene and polydiacetylenes. [30] As discussed earlier, a number of research groups have already successfully used the SOS theoretical three- and four-level models to describe the observed $\chi^{(3)}$ spectra of conjugated polymers; [10a, 25, 37-38, 54] molecular excitons are central to the SOS theory. Experimentally, site-selective fluorescence spectroscopy on *p*-phenylene vinylene polymers and oligomers has been used to show that the lowest energy optically allowed transitions in the absorption and emission spectra of these materials are excitonic in nature. [62b,c] We have similarly employed site-selective fluorescence spectroscopy to probe the excited states of the conjugated polyimines of chart 1 and confirm that they are best described as molecular excitons.

The conjugated aromatic polyimines (chart 1), unlike their isoelectronic *p*-phenylene vinylene polymers, are not highly fluorescent. The photoluminescence (PL) quantum efficiency of thin films of these polymers is only in the range of 10^{-3} to 10^{0}%, Nevertheless, excitation wavelength variation in PL studies of these materials has provided qualitative insights into their excited-state electronic structures. In our site-selective PL studies, the excitation wavelength was tuned between the absorption maximum (λ_{max}) and close to the absorption edge (E_g) of each polymer. The results are exemplified by those for PMOPI thin film in Figure 5 where the PL

spectra corresponding to excitation wavelength in the range of 450 to 540 nm are displayed. The PL emission maximum (588 nm) is unchanged between 450-500-nm excitation after which a progressive red shift of the emission λ_{max} with excitation wavelength is observed. The variation of emission energy with excitation energy of the PMOPI thin film shown in Figure 6 implies that the emission is not from a band-to band transition but a number of discrete states. Emission from a band-to-band transition would be completely independent of the excitation wavelength.[62b,c] Site-selective PL spectra, with excitation wavelength tuned from the absorption maximum to the absorption edge (Table 1), of the other polyimines were very similar to those of PMOPI except for the spectral shifts with the absorption and emission regions of each polymer. For example, compared to PMOPI which has excitation-independent emission maximum at 588 nm (2.11 eV), those of PPI, PBPI, and PHOPI were at 535 nm (2.32 eV), 565 nm (2.19 eV), and 624nm (1.99 eV), respectively. Interestingly, these results are also qualitatively similar to those observed on *p*-phenylene vinylene polymers. [62b,c]

A schematic illustration of the electronic structure of the conjugated polyimines is shown in chart 3. This picture is based on the results of the site-selective PL spectroscopy and similar prior excitonic description of other conjugated polymers. [54] The excited state structure of a conjugated polyimine, in this picture (chart 3), consists of some discrete excitonic states ($1B_u$, etc) with energy levels lying below the onset of the conduction band continum designated nB_u. Emission of the polymer can thus occur upon excitation with an energy less than E_{nBu} as well as with a higher energy. One of the discrete excitonic states lying between the $1B_u$ and nB_u levels is the non-emissive mA_g state, which has been revealed by two-photon absorption spectroscopy by others. [11, 54] The most important conclusions from the site-selective fluorescence spectroscopy of the conjugated polyimines are that excitonic description of their excited states is

justified and consequently that the sum-over-states (SOS) theoretical three-and four-level model descriptions of the third-order NLO response of the polyimines has experimental basis.

SOS Theoretical Model Analysis of $|\chi^{(3)}(-3\omega;\omega,\omega,\omega)|$ Spectra. A nonlinear parameter-estimation technique, the Levenberg-Marquardt method, [64] was used in our SOS theoretical model fitting of the $|\chi^{(3)}(-3\omega;\omega,\omega,\omega)|$ spectra. This technique incorporates a self-adjustable parameter in the computation scheme to perform root-finding iteration by using the inverse Hessian method and the steepest decent method. [64] It is very efficient for fitting experimental data with a highly nonlinear equation such as equations (2) to (4) in the present work.

The notation and physical meaning of the parameters in the 2-, 3-, and 4-level SOS models are listed in Table 2. As more levels are included, the SOS model equation (4) becomes much more complicated. There are three fitting parameters involved in the 2-level model, namely the energy level and the linewidth of $1B_u$ state and the transition dipole between the ground state ($1A_g$) and the $1B_u$ state. Going to the 3-level model doubles the number of the fitting parameters to six. All the parameters in the 2-level and 3-level models were obtained as the best estimates from fitting the dispersion data with the Levenberg-Marquardt algorithm. At the 4-level model, the additional B_u-type excited state is justified by the previously discussed site-selective fluorescence experiments that showed several discrete energy levels available for one-photon transition. To fit the $\chi^{(3)}$ dispersion data, the 4-level model requires a total of 10 fitting parameters, including 3 energy levels and their associated 3 linewidths and 4 transition dipole moments. Due to the complexity of solving the set of nonlinear equations involved in fitting the 4-level model to the $\chi^{(3)}$ spectra, some of the fitting parameters were either initially fixed at or guessed as the values obtained from the 3-level model. This ensured convergence of the fitting parameters to values that are consistent with physical meaning.

Figure 7 is an example of SOS model fitting of the $\chi^{(3)}$ spectrum of PPI by using the 2-, 3-, and 4-level models. An important observation is the progressive improvement on the agreement between the data and the model as more excited states are included in the SOS model. The experimental $|\chi^{(3)}(-3\omega;\omega,\omega,\omega)|$ dispersion of PPI departs considerably from the 2-level model prediction, suggesting that the simple consideration of band-to-band transition of the two-level model is not adequate for describing the cubic NLO response of this polymer. The 3-level model fails in giving a good fit at higher-energy regions especially around the resonant peak. The 3-level model fit of the $\chi^{(3)}$ spectrum of PPI reveals a mA_g state at 3.55 eV with a corresponding two-photon resonance at ~ 1.78 eV which differs by a huge amount from the observed resonance around ~1.28 eV. Good agreement between the data and the theory was achieved in the 4-level model. According to the 4-level model, the observed 0.93-eV resonance is the three-photon resonance of the $1B_u$ state (E_{1Bu}=2.79 eV) and the 1.28-eV resonance is due to the three-photon resonance of the nB_u state (E_{nBu}=3.85 eV). The 4-level SOS model for PPI also predicts a mA_g state lying at 3.65 eV whose two-photon resonance (~1.82 eV) is beyond the experimentally measured spectral range. It is interesting to note that the ordering of the $1B_u$, mA_g, and nB_u states in PPI is similar to that reported for the polydiacetylene P-4BCMU, indicating that the mA_g, state lies in between $1B_u$ and nB_u states.[54] However, the 4-level model does not describe the nonlinear optical response of all the polymers in the present study. In some $|\chi^{(3)}(-3\omega;\omega,\omega,\omega)|$ spectra, such as those of PBPI and PSPI, the 3-level model gives a good fit of the data in the whole spectral range and no improvement of the fit is achieved by going to the 4-level model.

In the following section , the experimental $\chi^{(3)}$ spectra for all the polymers in chart 1 will be presented along with their best fit by either the 3-level or 4-level theoretical model. The

fitting parameters of the best model fits are listed in Table 3. The 4-level model fit of the $|\chi^{(3)}(-3\omega;\omega,\omega,\omega)|$ dispersion of PMOPI revealed that the energy level of the nB_u state of PMOPI is 4.11 eV, which is considerably higher than the onset of the conduction band continuum (~2.45 eV) obtained from the steady-state site-selective fluorescence experiment. This discrepancy may be due to the large differences in the pulse width and intensity of the light sources employed in the two experiments, suggesting that the excited states that make significant contributions to fluorescence and nonlinear optical properties may be different for some polymers. However, comparison of the results of site-selective fluorescence spectroscopy and the theoretical fit of $|\chi^{(3)}(-3\omega;\omega,\omega,\omega)|$ dispersion data reveals a consistent picture that molecular exciton states are essential to the optical and nonlinear optical response of conjugated polymers in general and the conjugated polyimines in particular.

Effects of Structure on the Third-Order Nonlinear Optical Properties

Backbone Structure. The effects of variation of polymer backbone structure on the third-order optical nonlinearity are discernible from the comparison of the $|\chi^{(3)}(-3\omega;\omega,\omega,\omega)|$ spectra of PPI, PBPI, PSPI, and PBEPI shown in Figure 8. The solid lines shown in the figure are the theoretical fits: 4-level model for PPI; 3-level model for PBPI and PSI; and 2-level model for PBEPI. The theoretical models agree very well with the data. Unlike the $|\chi^{(3)}(-3\omega;\omega,\omega,\omega)|$ spectrum of PPI which clearly requires the 4-level model, the $|\chi^{(3)}(-3\omega;\omega,\omega,\omega)|$ spectra of PBPI and PSPI were well described by the 3-level model, which means that an A_g-type excited state coupled with the lowest-lying excited state ($1B_u$) are sufficient to describe the third-order nonlinear optical response of these two polymers, at least in the experimentally measured frequency range. In the case of the nonconjugated PBEPI, the 2-level model is the best fit of the

$|\chi^{(3)}(-3\omega;\omega,\omega,\omega)|$ data in accord with the single resonance feature observed in the measured spectral range.

The off-resonant third-order optical susceptibility at 0.52 eV (2.38 μm) of the parent conjugated polyimine, PPI, is 1.6×10^{-12} esu. The off-resonant $\chi^{(3)}$, measured at 0.52 eV, is 5.2×10^{-12}, 1.1×10^{-12}, and 1.0×10^{-12} esu for PBPI, PSPI, and PBEPI, respectively. A common feature of the four spectra in Figure 8 is the occurrence of a major resonant peak at about 1/3 of the lowest π-π^* transition energy observed in the optical absorption spectra of these polymers. Therefore, this resonance is assigned to the three-photon resonance of the $1B_u$ state. In all four cases, the three-photon resonance results in considerable enhancement of the third-order optical susceptibility. There is about a factor 10, 6.2, 8.6, and 4.5 increase of $\chi^{(3)}$ due to the three-photon resonance of PPI (1.6×10^{-11} esu), PBPI (3.2×10^{-11} esu), PSPI (9.5×10^{-12} esu), and PBEPI (4.5×10^{-12} esu), respectively. Compared to the $|\chi^{(3)}(-3\omega;\omega,\omega,\omega)|$ dispersion data of PPI, these results indicate that by changing every other *p*-phenylene linkage in PPI to *p*-biphenylene linkage the $\chi^{(3)}$values in the whole spectral range are increased by a factor of 2.0-3.2 in PBPI, but that similar introduction of stilbene linkage (PSPI) or biphenylene ether linkage (PBEPI) results in a considerable decrease of $\chi^{(3)}$.

Despite the factor of 1.37 lower molecular number density of PBPI compared to PPI, an enhancement of $\chi^{(3)}$ is observed in PBPI due to its large transition dipole moment between the $1A_g$ and $1B_u$ states (μ_{01}) compared to that of PPI (Table 3). Another interesting feature of the excited-state parameters of PBPI is the much smaller transition dipole moment between the $1B_u$ and mA_g states (μ_{12} =7.90 D) compared to that between $1A_g$ and the $1B_u$ states (μ_{01}=27.21 D) (Table 3). This huge difference in the two transition dipole moments appear to reduce the interference effect caused by the opposite signs of the two optical channels in 3-level materials.

The reduction of $\chi^{(3)}$ in PSPI compared to PPI is due to the reductions in both the number density and the transition dipole moment between the ground state and the one-photon excited state (Table 3). Although the optical bandgap of PSPI is smaller that that of PPI (Table 1), the relative magnitude of the $\chi^{(3)}$ values of these two polymers indicates that a smaller bandgap does not necessarily lead to increase of $\chi^{(3)}$. In fact, a similar finding has been reported by Marder et al. from the study of the second hyperpolarizability (γ) of conjugated molecules.[65] They showed that the optimal γ value occurs at a nonzero bond length alternation in a series of systematically designed molecules, which means that the largest γ was found not in the molecule with the smallest optical bandgap.[65] It is also interesting to note that the molecular structure of PSPI can be regarded as an *alternating copolymer* of PPI and PPV (poly(*p*-phenylene vinylene)). The optical bandgap of PSPI (E_g=2.38 eV) lies between those of PPI (E_g=2.50 eV) and PPV (E_g=2.34 eV).[66] PPV has been reported to have a large third-order optical nonlinearity ($\chi^{(3)}=7.8\times10^{-12}$ esu, THG at 1.85 μm). [17a] The smaller $\chi^{(3)}$ value of PSPI compared to both PPI and PPV indicates that the third-order optical nonlinearity of PSPI is lower than that of either constituent homopolymer. Comparison of the $\chi^{(3)}$ spectra of PBEPI and PPI shows that at off-resonance regions the $\chi^{(3)}$ of PBEPI is much smaller than that of PPI. Furthermore, the extent of three-photon resonance enhancement of the $\chi^{(3)}$ of PBEPI is far less than that of PPI and the other conjugated polyimines. These observations confirm that π-electron conjugation beyond a polymer repeat unit is required for large third-order optical nonlinearity. We also point out that the non-conjugated PBEPI is the only polymer among the polyimines investigated, which can be described by a two-level model.

Side-group Substitutions. The $|\chi^{(3)}(-3\omega;\omega,\omega,\omega)|$ spectra of PMOPI, PHOPI, and MO-PHOPI are shown in Figure 9 along with the spectrum of the parent PPI. The $\chi^{(3)}$ dispersion data of all

three substituted polymers, as well as PPI, are in very good agreement with the 4-level model description. A particularly interesting observation is the occurrence of three resonances in the $|\chi^{(3)}(-3\omega;\omega,\omega,\omega)|$ dispersion of PHOPI and MO-PHOPI. For this reason, only the 4-level model that consists of three excited states is capable of accounting for the three multiphoton resonances. For example, as shown from the 4-level fitting parameters of MO-PHOPI in Table 3, the $1B_u$, mA_g, and nB_u states lie at 2.21 eV, 2.58 eV, and 2.76 eV with corresponding resonances at 0.74 eV (three-photon), 1.29 eV (two-photon), and 0.92 eV (three-photon), respectively. These predicted resonances agree fairly well with the observed $\chi^{(3)}$ dispersion data. Although only two clear resonances are observed in the $\chi^{(3)}$ spectrum of PMOPI in the measured spectral range, the 4-level model was also the best fit of the data.

All the $\chi^{(3)}$ spectra in Figure 9 reveal a major resonance at about 1/3 of the lowest π-π^* transition energy observed in the optical absorption spectra, confirming its three-photon nature. The off-resonant $\chi^{(3)}$ magnitude, measured at 0.52 eV (2.38 μm), is 7.3×10^{-12}, 2.3×10^{-12}, and 1.6×10^{-11} esu, whereas the associated three-photon-resonance enhanced $\chi^{(3)}$ value is 5.2×10^{-11}, 1.1×10^{-11}, and 7.2×10^{-11} esu for PMOPI, PHOPI, and MO-PHOPI, respectively. About a factor of 4.5 increase of the off-resonance $\chi^{(3)}$value and a factor of 3.2 increase of the on-resonance $\chi^{(3)}$ value are observed in PMOPI compared to PPI. The enhancement of optical nonlinearity by the dimethoxy substitution in PMOPI compared to PPI may be explained by the greater electron delocalization and electron density in PMOPI as evidenced by its smaller π-π^* gap and larger absorption coefficient (Figure 2). However, such a correlation of increased $\chi^{(3)}$ with increased electron delocalization does not hold in the case of PHOPI. The $\chi^{(3)}$ of PHOPI was found to be much lower than that of PMOPI over the entire $\chi^{(3)}$ spectrum, contrary to expectations from its smaller bandgap. Intramolecular hydrogen bonding between the hydroxyl group and the imine

nitrogen results in greater electron delocalization and thus smaller bandgap in PHOPI compared to PMOPI (Figure 2, Table 1). However, the reduction in bandgap in going from PMOPI to PHOPI does not lead to any increase of $\chi^{(3)}$.

The methoxy derivatization of PHOPI gives rise to about an order of magnitude increase in the third-order optical susceptibility throughout the spectral range, as observed in the $\chi^{(3)}$ spectrum of MO-PHOPI, while having negligible effect on the lowest energy π-π^* optical transition (Table 1). Clearly, this dramatic enhancement of $\chi^{(3)}$ in going from PHOPI to MO-PHOPI cannot be explained by considerations of optical bandgap (E_g) and electron delocalization variations. We have also considered the possible role of excited state intramolecular proton transfer (ESIPT) on the NLO response of both PHOPI and MO-PHOPI. Although ESIPT (Scheme 1) is well-known to occur in intramolecular OH-bonded small molecules, oligomers, and some polymers,[67, 68] we have no evidence that it occurs in PHOPI or MO-PHOPI. Even if ESIPT occurs in PHOPI and MO-PHOPI as shown in scheme 1, it could not explain the observed order-of-magnitude difference in their $|\chi^{(3)}|$ spectra. Since the ESIPT process, i.e. formation of the excited ketone (K*) tautomer from the excited enol (E*) tautomer, occurs within 1ps of photoexcitation,[67] the excited species contributing to NLO response as probed by the 35-45ps THG would be the ketone tautomer (K*). It would be a significant discovery if it were to be the case that one and not the other exhibits ESIPT and that this difference is the origin of the large NLO enhancement in MO-PHOPI compared to PHOPI. However, ESIPT likely does not occur in either polymer because of the known inhibition of the process by large electronic delocalization in conjugated rigid-chain polymers.[68]

The simple methoxy derivatization in going from PHOPI to MO-PHOPI has a remarkable effect on the excited state structure as evidenced by comparing the relevant transition

dipole moments in Table 3. Although the number density is reduced 11% by the methoxy appendage, μ_{01} is increased by 75% and, μ_{12} is more than doubled in going from PHOPI to MO-PHOPI. This means that periodic *electron density modulation* along the main chain is dramatically different between these two donor side-group substituted polymers even though the overall electronic delocalization (ground state electronic structure) is nearly identical. The donor side-group substitutions in MO-PHOPI are *asymmetric* and hence also the associated electron density modulation along the chain, compared to the *symmetric* PHOPI and PMOPI cases. We believe that these differences in molecular and electronic structures best account for the large differences in third-order optical properties. A recent theoretical study [33] of the effects of donor side groups on the third-order nonlinear optical susceptibility of conjugated polymers appears to provide support of our interpretation. Although the theory was expressed in the language of *semiconductor superlattices (minibands, minigaps, etc.)*, rather than in molecular terms, the main theoretical result is that variation in the *arrangement* of donor side groups along a conjugated polymer chain can result in dramatic changes in the electronic band structure and large enhancements of $\chi^{(3)}$. The calculations show that side groups that are appended along the conjugated polymer chain induce a *superlattice potential*, whose periodicity depends on the arrangement of the side-groups, in addition to the lattice potential of the underivatized parent chain.[33] What is intriguing is whether the minibands of the exact theory [33] are similar to the discrete excited states ($1B_u$, mA_g, etc) of the semiempirical SOS models. Further theoretical and experimental studies of the effects of side groups on third-order optical response of polymers are highly desired to clarify these issues.

Random Copolymerization. The third-order optical susceptibility $\chi^{(3)}(-3\omega;\omega,\omega,\omega)$ spectra of PMPI and PPI/PMPI thin films are shown in Figure 10 along with that of PPI for comparison.

The solid lines in the figure are the theoretical fits by the 3-level model for PMPI and the 4-level model for PPI and the random copolymer PPI/PMPI, respectively. The agreement between the theoretical models and the experimental $\chi^{(3)}$ dispersion data is fairly good.

The methyl derivative PMPI, and the random copolymer PPI/PMPI which contains 53 mol % PPI, exhibit an off-resonant $\chi^{(3)}$ value at ~0.52 eV (2.38 μm) of 0.93×10^{-12} and 2.3×10^{-12} esu, respectively. These $\chi^{(3)}$ dispersion data, similar to that of PPI, also reveal a resonant feature that can be attributed to dispersion processes since the optical absorption spectra of these polymers do not show any absorption features beyond 0.6 μm (i.e. $h\nu < 2.07$ eV, Figure 3). The resonant peak at ~0.93 eV, which is about 1/3 of the energy of the lowest π-π^* transition, is therefore assigned to the three-photon resonance. The magnitude of the three-photon resonance enhanced $\chi^{(3)}$ value of PMPI and PPI/PMPI is 6.4×10^{-12} and 1.9×10^{-11} esu, respectively. Compared to the off-resonant $\chi^{(3)}$ value of these two polymers, three-photon resonance results in a factor of 7-8 enhancement of the NLO response.

Although PPI, its methyl derivative PMPI, and their random copolymer PPI/PMPI (53 mol % PPI) all have identical optical absorption λ_{max} and bandgap (Figure 3 and Table 1), they all have significantly different third-order optical susceptibility. The methyl side group on every other *p*-phenylene ring of PMPI has a profound influence on the $\chi^{(3)}$ spectrum, resulting in a factor of 1.72 – 2.50 reduction in optical nonlinearity throughout the spectral range investigated. This major adverse change in optical nonlinearity in going from PPI to PMPI is obviously not due to the rather small(<9%) decrease in number density of polymer molecules with methyl appendage (Table 3). The main reason for the decline in the $\chi^{(3)}$ of PMPI relative to PPI is the large transition dipole moment (μ_{12} = 27.38 D) connecting the first two-excited states, making

PMPI a three-level material in which interference occurs between the two optical channels contributing to $\chi^{(3)}$.

It is interesting that both the off-resonance and on-resonance $\chi^{(3)}$ values of the random copolymer PPI/PMPI are enhanced compared to the parent homopolymers, especially PPI. As expected, the number density of PPI/PMPI is the compositional average of the number densities of the parent homopolymers and hence the observed enhancement of optical nonlinearity in PPI/PMPI reflects entirely on favorable changes in the excited-state electronic structure relative to the homopolymers. The most notable of these changes are the factors of 2 and 2.5 increases in the transition dipole moments μ_{03} and μ_{12}, respectively, in going from PPI to the random copolymer. These features of the electronic excited-state structure of PPI/PMPI (53 mol % PPI) are due to its disordered, non-periodic, chain structure, which implies lack of centrosymmetry.

Transition Dipole Moments. Our use of the SOS theoretical models to fit the $\chi^{(3)}$ spectra of these polymers is clearly phenomenological in nature. Therefore, the resulting fitting parameters, especially the transition dipole moments μ_{ij} shown in Table 3, must not be regarded as absolute and accurate description of the electronic structure of the polymers. Integration of the optical absorption spectrum provided an estimate of one of the transition dipole moments for comparison with computed values. The transition dipole moment of the lowest energy π-π^* electronic transition was estimated by integration of the optical absorption according to the following relation:[69]

$$\mu^2 = \frac{2.401x10^{-3}}{N}\int_{transition}\frac{n\alpha d\lambda}{\lambda} \qquad (6)$$

The transition dipole moment μ in this expression is in Debye (D), N is the number density of polymer repeat unit in 10^{21} cm^{-3}, and α is the absorption coefficient in cm^{-1}.

The estimated transition dipole moment (μ_{01}) for each polymer is listed in Table 3. Only in two cases, PHOPI and PSPI, which have relatively small $\chi^{(3)}$ values, is the computed μ_{01} close to the experimentally estimated one. Although the μ_{01} data in the range 8.56 – 12.17 D are also approximate values, the fitting parameter values are significantly larger. The major reason for the much larger computed μ_{01} values compared to the experimental estimates is the fact that only a few excited states are included in the SOS models. Including more excited states in an SOS model gives rise to smaller computed transition dipole moments as demonstrated by comparing the parameters of the four-level model to the three- and two-level models in the present work (Table 3) and those reported for other polymers.[22, 38] Another important reason for the deviation between the computed μ_{01} and its experimental estimate is the use of the repeat unit number density in equation (6) for estimating μ and in equation (4) for calculating the macroscopic $\chi^{(3)}$ from the second hyperpolarizability. Since electron delocalization most likely extends over several repeat units, the true number density will be smaller than that used in equation (6) and the experimental μ will increase as $(1/N)^{1/2}$. Similarly the transition dipole moments computed by SOS model fitting will change with number density as $(1/N)^{1/4}$. All these considerations suggest that the fitting parameters, particularly the transition dipole moments, obtained by the SOS theoretical analysis of $\chi^{(3)}$ spectra should only be regarded as an approximate description of the electronic structure of the materials. However, the fitting parameters and the approximate electronic structure they describe can still provide a basis for the qualitative elucidation of the nonlinear optical response and the structure -$\chi^{(3)}$ trends in the same class of polymers.

Predictions of the SOS Models. The SOS theoretical model fitting parameters obtained by analysis of $\chi^{(3)}(-3\omega;\omega,\omega,\omega)$ can provide a wealth of information about the NLO response of a material. One relevant information of interest is the *static* or *zero-frequency* ($\omega = 0$) third-order optical susceptibility. These zero-frequency $\chi^{(3)}$ values are calculated for the SOS models investigated here by nullifying damping coefficients in the time-dependent perturbation equation (equation (2)) while taking ω=0:

2-level model:
$$\chi^{(3)} = \frac{-NL_f^4\mu_{01}^4}{5\hbar^3\omega_{01}^3}; \quad L_f = \frac{n^2+2}{3} \tag{7}$$

3-level model:
$$\chi^{(3)} = \frac{NL_f^4\mu_{01}^2}{5\hbar^3\omega_{01}^2}\left(\frac{\mu_{12}^2}{\omega_{02}} - \frac{\mu_{01}^2}{\omega_{01}}\right) \tag{8}$$

4-level model:
$$\chi^{(3)} = \frac{NL_f^4}{5\hbar^3}\left(\frac{\mu_{01}^2\mu_{12}^2}{\omega_{01}^2\omega_{02}} + \frac{\mu_{03}^2\mu_{23}^2}{\omega_{03}^2\omega_{02}} + \frac{2\mu_{01}\mu_{12}\mu_{03}\mu_{23}}{\omega_{01}\omega_{02}\omega_{03}} - \frac{\mu_{01}^4}{\omega_{01}^3} - \frac{\mu_{03}^4}{\omega_{03}^3} - \frac{\mu_{01}^2\mu_{03}^2}{\omega_{01}^2\omega_{03}} - \frac{\mu_{01}^2\mu_{03}^2}{\omega_{01}\omega_{03}^2}\right) \tag{9}$$

In these expressions, L_f is the Lorentz-Lorenz local field correction factor, n is the far-off-resonance refractive index, and the notation of the other parameters is listed in Table 2. A distinct feature of the 2-level model for a centrosymmetric conjugated polymer is its *negative* zero-frequency $\chi^{(3)}$ as represented in equation (7). Depending on the relative magnitudes of μ_{01} and μ_{12}, the zero-frequency $\chi^{(3)}$ of a 3-level polymer can be either positive or negative. If μ_{01} is

larger than μ_{12}, $\chi^{(3)}$ will be negative whereas it is positive otherwise. Because of the existence of the two opposite contributions, it has been suggested that an interference effect can be expected to result in the lowering of the third-order optical susceptibility in 3-level materials compared to 2-level materials.[22, 38] A 4-level model with more excited states has more optical channels contributing to the NLO response. A consequence of this as seen in equation (9) is that enhancement of the third-order susceptibility may result. This is exemplified by the fact that the polymers with the highest $\chi^{(3)}$ investigated in the present study are all best described by the 4-level model.

The calculated zero-frequency $\chi^{(3)}$ along with the three-photon resonance-enhanced and off-resonant (at 0.52 eV) $\chi^{(3)}$ of the series of conjugated polyimines are collected in Table 4. All the predicted zero-frequency $\chi^{(3)}$ values have negative sign, except PSPI, indicating that 4-level materials, similar to 2-level materials, are endowed with a negative static $\chi^{(3)}$. This is understandable from the dominant negative terms in equation (9), including the third term (see Table 3). A small positive $\chi^{(3)}$ is predicted for PSPI, indicative of interference effects between the positive and negative terms in a 3-level material. Comparison of the magnitude of the predicted zero-frequency $\chi^{(3)}$ to the measured off-resonant $\chi^{(3)}$ at 2.38 μm (0.52 eV) shows two important features (Table 4). First, the predicted and measured $\chi^{(3)}$ values are surprisingly very close, with the measured (2.38-μm) values being higher. Second, the predicted relative ordering of the magnitude of $\chi^{(3)}$ is essentially the same as that measured at 2.38 μm for the series of polymers. These results suggest that although the electronic structure parameters extracted by the SOS models are approximate (Table 3), they are nevertheless quite satisfactory in giving insights into the NLO response of a series of conjugated polymers.

The SOS model makes possible the deconvolution of the magnitude of the frequency-dispersed third-order optical susceptibility $|\chi^{(3)}(-3\omega;\omega,\omega,\omega)|$, measured by THG spectroscopy, into the real and imaginary components as well as the prediction of the other third-order NLO processes such as $\chi^{(3)}(-\omega;\omega,-\omega,\omega)$ determined by degenerate four wave mixing (DFWM). Intensity-dependent refractive index which is of interest in all-optical switching is related to $\chi^{(3)}(-\omega;\omega,-\omega,\omega)$. Frequency-dispersed $\chi^{(3)}(-\omega;\omega,-\omega,\omega)$ by DFWM spectroscopy has not been reported for conjugated polymers because of the greater experimental difficulty compared to the measurement of $\chi^{(3)}(-3\omega;\omega,\omega,\omega)$ by THG spectroscopy.[10, 12a, 21-23, 54] Figure 11 shows the 4-level model prediction of the real and imaginary components along with the magnitude of $\chi^{(3)}(-3\omega;\omega,\omega,\omega)$ for PPI. Re $[\chi^{(3)}]$ is seen to change sign from negative to positive at a frequency around 1/3 E_{1Bu} (~ 0.90 eV) and changes sign again at about 1/3 E_{nBu} (~ 1.30 eV). Accordingly, Im $[\chi^{(3)}]$ shows resonances at these two frequencies. Thus for all wavelengths greater than 1.38 μm (0.90 eV), Re$[\chi^{(3)}]$ is *negative* for the parent conjugated polyimine PPI. In fact, all the $|\chi^{(3)}(-3\omega;\omega,\omega,\omega)|$ spectra of the different polymers could be deconvoluted into their real and imaginary components, leading to similar results and conclusions.

The $\chi^{(3)}(-\omega;\omega,-\omega,\omega)$ spectrum of each conjugated polyimine was predicted by using the time-dependent SOS perturbation expression (equation (2)) in combination with a frequency mixing format that is different from that for THG.[47,48] A distinct feature of the $\chi^{(3)}(-\omega;\omega,-\omega,\omega)$ spectrum is that it exhibits only one-photon and two-photon, but not three-photon, resonances. Based on the same electronic structure parameters in Table 3, obtained from SOS model fitting of $|\chi^{(3)}(-3\omega;\omega,\omega,\omega)|$ spectra, the $\chi^{(3)}(-\omega;\omega,-\omega,\omega)$ spectra of the polymers were predicted and found to exhibit greater resonance enhancements compared to the measured $\chi^{(3)}(-3\omega;\omega,-\omega,\omega)$ spectra. The results are exemplified by Figure 12 which shows the $\chi^{(3)}(-\omega;\omega,-\omega,\omega)$ spectra of

MO-PHOPI predicted by the 4-level model. The $Re[\chi^{(3)}(-\omega;\omega,-\omega,\omega)]$ spectrum, which is related to the intensity-dependent refractive index ($n=n_0+n_2I$), is seen to be negative throughout the spectral range, indicating that this material exhibits *self-defocusing action*. The resonances in the $\chi^{(3)}(-\omega;\omega,-\omega,\omega)$ spectra of Figure 12 can be assigned as follows: two-photon resonance of the mA_g state is at ~1.30 eV; one-photon resonances of the $1B_u$ state (E_{1Bu} = 2.21 eV) are at ~2.05 and ~2.35 eV; and one-photon resonance of the nB_u state (E_{nBu} = 2.76 eV) is at ~2.70 eV. Due to these multiple one-photon and two-photon resonances, the $\chi^{(3)}(-\omega;\omega,-\omega,\omega)$ spectra reveal more pronounced resonance-enhanced $\chi^{(3)}$ values than found in the measured $|\chi^{(3)}_{THG}|$ spectrum. For example, the resonance-enhanced magnitude of $\chi^{(3)}(-\omega;\omega,-\omega,\omega)$ was in the range of 0.12 – 4.2×10^{-9}esu for the series of polyimines compared to 0.45 – 7.2 x 10^{-11}esu observed for resonance-enhanced $\chi^{(3)}_{THG}$ (Table 4). The almost two orders of magnitude difference between observed $\chi^{(3)}_{THG}$ and predicted $\chi^{(3)}_{DFWM}$ values for the same polymers reflects their origins in different frequency mixing processes and underscores the potential difficulty in comparing the $\chi^{(3)}$ values of different conjugated polymers reported in the literature. Equally important is the observation that resonances in the nonlinear optical response probed by DFWM cover a much broader spectral range than expected from the optical absorption spectrum. For example, off-resonance $\chi^{(3)}$ values are only obtained in Figure 12 when $h\nu < 1.2$ eV which is much smaller than the optical absorption edge of MO-PHOPI (E_g = 2.03 eV).

Conclusions

The frequency dispersed third-order nonlinear optical properties of a series of systematically derivatized conjugated aromatic polyimines have been measured by THG spectroscopy over a wide spectral range and analyzed by theoretical SOS models. The results

clearly show that this class of conjugated polymers has a large nonlinear optical response that is tunable by side-group substitutions, random copolymerization, and backbone variation. Among the series of polymers, an asymmetric substituted polymine, MO-PHOPI, was found to have the largest optical nonlinearity with off-resonant (at 2.4 μm; 0.52 eV) and three-photon resonance-enhanced $\chi^{(3)}$ values of 1.6×10^{-11} and 7.2×10^{-11} esu, respectively, which are about an order of magnitude enhanced compared to the parent, non-substituted, PPI. No relationship between the magnitude of $\chi^{(3)}$ and the energy of the lowest π-π^* optical gap (E_g) which was in the range of 2.03-2.83 eV, was found. The good agreement between three- and four-level theoretical SOS models and the observed frequency dispersed $\chi^{(3)}$ data and multiphoton resonances in the $\chi^{(3)}$ spectra confirmed the critical roles of two to three excited-state levels in the nonlinear optical response of this class of conjugated polymers. The large variation of third-order optical nonlinearity with molecular structure of these polymers can thus be traced to the dramatic changes in the excited-state electronic structure of the materials. The findings that random copolymerization and asymmetric side-group substitutions on a conjugated polymer can lead to large enhancements of optical nonlinearity, suggest that these approaches are promising new directions for optimizing third-order optical polymers.

The three- and four-level SOS models have also allowed us to deconvolute the real and imaginary parts of the THG-measured $|\chi^{(3)}|$ spectra as well as to predict the $\chi^{(3)}$ $(-\omega;\omega,-\omega,\omega)$ spectra of the series of polymers, thus providing more insights into the different third-order nonlinear optical properties of the materials. Of particular significance is prediction of *negative* zero-frequency $\chi^{(3)}$ for all the polyimines investigated, except PSPI, which has a positive value. Furthermore, $\mathrm{Re}[\chi^{(3)}(-3\omega;\omega,\omega,\omega)]$ and $\mathrm{Re}[\chi^{(3)}(-\omega;\omega,-\omega,\omega)]$ were also negative for the same eight conjugated polymers over a wide spectral range that is off-resonant. This means that these

polymers will exhibit *self-defocusing phenomenon*, which is rare in organic molecules and polymers.[31b, 70] The predicted $\chi^{(3)}$ (-ω;ω,-ω,ω) spectra of the materials showed two-photon and one-photon enhanced $\chi^{(3)}$ values in the range of 0.12-4.2x10^{-9} esu which are significantly larger than those measured by THG spectroscopy. It is therefore important to measure both the magnitude and sign of $\chi^{(3)}$ (-ω;ω,-ω,ω) in future work for comparison with these predictions.

Acknowledgements

Work at the University of Rochester was supported by the National Science Foundation (Grants CHE-912-0001 and CTS-9311741) and in part by the Office of Naval Research.

References

(1) (a) Gibbs, H. M.; Khitrova, G.; Peygambarian, N., Eds. *Nonlinear Photonics,* Springer-Verlag: New York, **1990**; (b) Agrawal, G. P.; Boyd, R. W., Eds. *Contemporary Nonlinear Optics*, Academic Press: Boston, **1992**; (c) Sauteret, C.; Hermann, J.-P.; Frey, R.; Pradere, F.; Ducuing, J.; Baughman, R. H.; Chance, R. R. *Phys. Rev. Lett.* **1976**, *36*, 956-959.

(2) (a) Jenekhe, S. A.; Wynne, K. J., Eds. *Photonic and Optoelectronic Polymers*, American Chemical Society: Washington, DC, **1997**; (b) Jenekhe, S. A., Ed. *Macromolecular Host-Guest Complexes : Optical, Optoelectronic, and Photorefractive Properties and Applications,* Material Research Society : Pittsburgh, **1992**.

(3) (a) *Nonlinear Optical Properties of Organic Materials*, Proceedings of SPIE, Vol. 3147, in press (**1997**);(b) Hornak. L. A., Ed. *Polymers for Lightwave and Integrated Optics : Technology and Applications*, Marcel Dekker : New York, **1992**; (c) Marder, S. R.; John, J. E.; Stucky, G. D. Eds. *Materials for Nonlinear Optics : Chemical Perspectives,* American Chemical Society : Washington, DC, **1991**; (d) Brédas, J. L.; Silbey, R. Eds. *Conjugated Polymers : The Novel Science and Technology of Highly Conductive and Nonlinear Optically Active Materials,* Kluwer Academic Publishers: Dordrecht, The Netherlands, **1991**; (e) Prasad, P. N.; William, D. J. *Introduction to Nonlinear Optical Effects in Molecules and Polymers*, John Wiley : New York, **1991**; (f) Brédas, J. L.; Chance, R. R., Eds. *Conjugated Polymeric Materials : Opportunity in Electronics, Optoelectronics, and Molecular Electronics*, Klumer Academic Publishers: Dordrecht, The Netherlands, **1990**; (g) Messier, J.; Kajzar, F.; Prasad, P.; Ulrich, D., Eds. *Nonlinear Optical Effects in Organic Polymers*, Kluwer Academic Publishers: Dordrecht, The Netherlands, **1989**.

(4) Chemla, D. S.; Zyss, J., Eds. *Nonlinear Optical Properties of Organic Molecules and Crystals*, Vols.1 and 2, Academic Press : New York, **1987.**

(5) Brédas, J.J.; Adant, C.; Tackx, P.; Persoons, A.; Pierce, B. M. *Chem. Rev.* **1994,** *94*, 243-278.

(6) Fischer, G. L.; Boyd, R. W.; Gehr, R. J.; Jenekhe, S. A.; Osaheni, J. A.; Sipe, J. E.; Weller-Brophy, L. A. *Phys. Rev. Lett.* **1995,** *74*, 1871-1874.

(7) (a) Dalton, L.R. *Nature* **1992**, *359*, 269; (b) Dalton, L.R.; Sapochak, L. S.; Yu, L., *J. Phys. Chem.* **1993**, *97*, 2871-2883. (c) Rodenberger, D. C.; Heflin, J. R.; Garito, A.

F. *Nature* **1992**, *359*, 309-311; (d) Rodenberger, D. C.; Heflin, J. R.; Garito, A. F. *Phys. Rev A.* **1995**, *51*, 3234-3245.

(8) (a) Marder, S. R.; Torruellas, W. E.; Blanchard-Desce, M.; Ricci, V.; Stegmen, G. I.; Gilmour, S.; Brédas, J. L.; Li, J.; Bublitz, G. U.; Boxer, S. G. *Science* **1997**, *276*, 1233-1236; (b) Marder, S. R.; Gorman, C. B.; Meyers, F,; Perry, J. W.; Bourhill, G.; Brédas, J. L.; Pierce, B. M. *Science* **1994**, *265*, 632-635; (c) Meyers, F.; Marder, S. R.; Pierce, B. M.; Brédas, J. L. *J. Am. Chem. Soc.* **1994**, *116*, 10703-10714.

(9) (a) Craig, G. S. W.; Cohen, R. E.; Schrock, R. R.; Silbey, R. J.; Puccetti, G.; Ledoux, I.; Zyss, J. *J. Am. Chem. Soc.* **1993**, *115*, 860-867; (b) Samuel, I. D. W.; Ledoux, I.; Dhenaut, C.; Zyss, J.; Fox, H. H.; Schrock, R. R.; Sibley, R. J. *Science* **1994**, *265*, 1070-1072.

(10) (a) Torruellas, W. E.; Neher, D.; Zanoni, R.; Stegeman, G. I.; Kajzar, F.; Leclerc, M.. *J. Opt. Soc.Am. B* **1995**, *12*, 882-888; (b) Murato, H.; Takada, N.; Tsutsui, T.; Saito, S.; Kurihara, T.; Kaino, T. *J. Appl. Phys.***1991**, *70*, 2915-2920.

(11) Lawrence, B.; Torruellas, W. E.; Cha, M.; Sundheimer, M. L.; Stegeman, G. I.; Meth, J.; Etemad, S.; Baker, G. *Phys. Rev. Lett.* **1994**, *73*, 597-600.

(12) (a) Fann, W.-S.; Benson, S.; Madey, J. M. J.; Etemad, S.; Baker, G. L.; Kajzar, F. *Phys. Rev. Lett.* **1989**, *62*, 1492-1495. (b) Vijaya, R.; Murti, Y. V. G. S.; Rae, T. A. P.; Sundararajan, G. *J. Appl. Phys.* **1991**, *69*, 3429-3431.

(13) Kanetake, T.; Ishikawa, K.; Hasegawa, T.; Koda, T.; Takeda, K.; Hasegawa, M.; Kubodera, K.; Kobayashi, H. *Appl. Phy. Lett.* **1989**, *54*, 2287-2289.

(14) (a) Kaino, T.; Kobayashi, H.; Kubodera, K.-I.; Kurihara, T.; Saito, S.; Tsutsui, T.; Tokito, S. *Appl. Phys. Lett.* **1989**, *54*, 1619-1621. (b) Rao, D. N.; Chopra, P.; Ghoshal, S. K.; Swiatkiewicz, J.; Prasad. P. N. *J. Chem. Phys* . **1986**, *84*, 7049.

(15) (a) Swiatkiewicz, J.; Prasad, P. N.; Karasz, F. E.; Druy, M. A.; Glatkowski, P. *Appl. Phy. Lett.* **1990**, *56*, 892-894. (b) Sugiyama, T.; Wada, T.; Sasabe, H. *Synth. Met.* **1989**, *28*, C323. (c) Kaino, T.; Kubodera, K.; Kobayashi, H.; Kurihara, T.; Saito, S.; Tsutsui, T.; Tokito, S.; Murata, H. *Appl. Phys. Lett.* **1988**, *53*, 2002-2004.

(16) Houlding, V. H.; Nahata, A.; Yardley, J. T.; Elsenbaumer, R. L. *Chem. Mater.* **1990**, *2*, 169-172.

(17) (a) Kaino, T.; Kubodera, K.-I.; Tomaru, S.; Kurihara, T.; Saito, S.; Tsutsui, T.; Tokito, S. *Electronics Lett.* **1987**, *23*, 1095-1097. (b) Bubeck, G.; Kaltbeitzel, A.; Lenz, R. W.; Neher, D.; Stenger-Smith, J. D.; Wegner, G. in ref. 3c, p 143. (c) Mathy, A.; Ueberhofen, K.; Schenk, R.; Gregorius, H.; Garay, R.; Müllen, K.; Bubeck, C. *Phys. Rev. B.* **1996**, *53*, 4367-4376.

(18) Lee, C. Y.-C.; Swiatkiewicz, J.; Prasad, P. N.; Metha, R.; Bai, S. J. *Polymers* **1991**, *32*, 1195-1199.

(19) (a) Yu, L. P.; Dalton, L. R. *Synth. Met.* **1989**, *29*, E463-E470. (b) Yu, L. P.; Dalton, L. R. *Macromolecules* **1990**, *23*, 3439-3444.

(20) (a) Lindle, J. R.; Bartoli, F. J.; Hoffman, C. A.; Kim, O.-K.; Lee, Y. S.; Shirk, J. S.; Kafafi, Z. H. *Appl. Phys. Lett.* **1990**, *56*, 712-714. (b) Yu, L. P.; Chen, M.; Dalton, L. R. *Chem. Mater.* **1990**, *2*, 649-659.

(21) (a) Osaheni, J. A.; Jenekhe, S. A.; Vanherzeele, H.; Meth, J. S. *Chem. Mater.* **1991**, *3*, 218-221. (b) Agrawal, A. K.; Jenekhe, S. A.; Vanherzeele, H.; Meth, J. S. *Chem. Mater.* **1991**, *3*, 765-768. (c) Jenekhe, S. A.; Yang, C. J.; Vanherzeele, H.; Meth, J. S. *Chem. Mater.* **1991**, *3*, 985-988.

(22) (a) Agrawal, A. K.; Jenekhe, S. A.; Vanherzeele, H.; Meth, J. S. *J. Phys. Chem.* **1992**, *96*, 2837-2843. (b) Osaheni, J. A.; Jenekhe, S. A.; Vanherzeele, H.; Meth, J. S.; Sun, Y.; MacDiarmid, A. G. *J. Phys. Chem.* **1992**, *96*, 2830-2836.

(23) Jenekhe, S. A.; Osaheni, J. A.; Meth, J. S.; Vanherzeele, H. *Chem. Mater.* **1992**, *4*, 683-687.

(24) Messier, J. in reference 3g, p. 47-60.

(25) (a) Torruellas, W. E.; Neher, D.; Zanoni, R.; Stegeman, G. I.; Kajzar, F.; Leclerc, M. *Chem. Phys. Lett.* **1990**, *175*, 11-16. (b) Torruellas, W. E.; Rochford, K. B.; Zanoni, R.; Aramaki, S.; Stegeman, G. I. *Optics Commun.* **1991**, *82*, 94-100. (c) Aramaki, S.; Torruella, W.; Zanoni, R.; Stegeman, G. I. *Optics Commun.* **1991**, *85*, 527-535.

(26) (a) Agrawal, G. P.; Cojan, C.; Flytzanis, C. *Phys. Rev. B* **1978**, *17*, 776-789; (b) Rustagi, K. C.; Ducuing, J. *Optics Commun.* **1974**, *10*, 258-261. (c) Mehendale, S. C.; Rustagi, K. C. *Optics Commun.* **1979**, *28*, 359-362.

(27) Flytzanis, C. in ref. (4), pp. 121-135.

(28) (a) Zhao, M. T.; Singh, B. P.; Prasad, P. N. *J. Chem. Phys.* **1988**, *89*, 5535-5541. (b) Prasad, P. N.; Perrin, E.; Samoc, M. *J. Chem. Phys.* **1989**, *91*, 2360-2365. (c) Zhao, M. T.; Samoc, M.; Singh, B. P.; Prasad, P. N. *J. Phys. Chem.* **1989**, *93*, 7916-7920.

(29) Heflin, J. R.; Wong, K. Y.; Zamani-Khamiri, O.; Garito, A. F. *Phys. Rev. B* **1988**, *38*, 1573-1576.

(30) (a) Mukamel, S.; Wang, H. X. *Phys. Rev. Lett.* **1992**, *69*, 65-68. (b) Wang, H. X.; Mukamel, S. *J. Chem. Phys.* **1992**, *97*, 8019-8036.

(31) (a) Pierce, B. M. *Proc. SPIE* **1991**, *1560*, 148-161; (b) Dirk, C. W.; Herndon, W. D.; Cervantes-Lee, F.; Selnau, H.; Martinex, S.; Kalamegham, P.; Tan, A.; Campos,

G.; Velez, M.; Zyss, J.; Ledoux, I.; Cheng, L. T. *J. Am. Chem. Soc.* **1995**, *117*, 2214-2225.

(32) (a) Reinhardt, B. A.; Unroe, M. R.; Evers, R. C.; Zhao, M.; Samoc, M.; Prasad, P. N.; Sinsky, M. *Chem. Mater.* **1991**, *3*, 864-871. (b) Zhao, M.; Samoc, M.; Prasad, P. N.; Reinhardt, B. A.; Undoe, M. R.; Prazak, M.; Evers, R. C.; Kane, J. J.; Jariwala, C.; Sinsky, M. *Chem Mater.* **1990**, *2*, 670-678.

(33) Margulis, Vl. A.; Tomilin, O. B. *Synth. Met.* **1996**, *79*, 207-214.

(34) (a) Osaheni, J. A.; Jenekhe, S. A. *J. Am. Chem. Soc.* **1995**, *117*, 7389-7398; (b) Chen, X. L.; Jenekhe, S. A. *Macromolecules* **1996**, *29*, 6189-6192

(35) (a) Jenekhe, S. A.; Johnson, P. O.; Agrawal, A. K. *Macromolecules* **1989**, *22*, 3216-3222. (b) Jenekhe, S. A.; Johnson, P. O. *Macromolecules* **1990**, *23*, 4419-4429. (c) Roberts, M. F.; Jenekhe, S. A. *Chem. Mater.* **1990**, *2*, 224-226. (d) Roberts, M. F.; Jenekhe, S. A. *Chem. Mater.* **1990**, *2*, 629-631. (e) Roberts, M. F.; Jenekhe, S. A. *Macromolecules* **1991**, *24*, 3142-3146.

(36) (a) Yang, C. J.; Jenekhe, S. A. *Chem. Mater.* **1991**, *3*, 878-887. (b) Yang, C. J.; Jenekhe, S. A. *Macromolecules* **1995**, *28*, 1180-1196.

(37) Vanherzeele, H.; Meth, J. S.; Jenekhe, S. A.; Roberts, M. F. *J. Opt. Soc. Am. B* **1992**, *9*, 524-533.

(38) Meth, J. S.; Vanherzeele, H.; Jenekhe, S. A.; Yang. C. J.; Roberts, M. F.; Agrawal, A. K. *SPIE Proceedings* **1991**, *1560*, 13-24.

(39) Morgan, P. W.; Kwolek, S. L.; Pletcher, T. C. *Macromolecules* **1987**, *20*, 729-739.

(40) Swanepoel, R. *J. Opt. Soc. Am. A* **1985**, *2*, 1339-1343.

(41) (a) Manifacier, J. C.; Gasiot, J.; Fillard, J. P. *J. Phys. E : Sci. Instrum.* **1976**, *9*, 1002-1004. (b) Manifacier, J. C.; DE Murcia, M.; Fillard, J. P. *Thin Solid Films* **1977**, *41*, 127-135.

(42) (a) Yang, C. J.; Jenekhe, S. A. *Chem. Mater.* **1994**, *6*, 196-203; (b) Yang, C. J., Jenekhe, S. A. *Chem. Mater.* **1995**, *7*, 1276-1285.

(43) Vanherzeele, H. *Appl. Optics* **1990**, *29*, 2246-2258.

(44) Bethune, D. S. *J. Opt. Soc. Am. B* **1989**, *6*, 910-916.

(45) Neher, D.; Wolf, A.; Bubeck, C.; Wegner, G. *Chem. Phys. Lett.* **1989**, *163*, 116-122.

(46) Buchalter, B.; Meredith, G. R. *Appl. Optics* **1982**, *21*, 3221-3224.

(47) Orr, B. J.; Ward, J. F. *Mol. Phys.* **1971**, *20*, 513-526.

(48) Langhoff, P. W.; Epstein, G. W.; Karplus, M. *Rev. Mod. Phys.* **1972**, *44*, 602-644.

(49) Kuzyk, M. G.; Dirk, C. W. *Phys. Rev. A* **1990**, *41*, 5098-5109.

(50) Dixit, S. N.; Guo, D.; Mazumdar, S. *Mol. Cryst. Liq. Cryst.* **1991**, *194*, 33-41.

(51) Soos, Z. G.; McWilliams, P. C. M.; Hayden, G. W. *Chem. Phys. Lett.* **1990**, *171*, 14-18.

(52) McWilliams, P. C. W.; Hayden, G. W.; Soos, Z. G. *Phys. Rev. B* **1991**, *43*, 9777-9791.

(53) Wu, J. W.; Heflin, J. R.; Norwood, R. A.; Wong, K. Y.; Zamani-Khamir, O.; Garito, A. F. *J. Opt. Soc. Am. B* **1989**, *6*, 707-720.

(54) (a) Guo, D.; Mazumdar, S.; Stegeman, G. I.; Cha, M.; Neher, D.; Aramaki, S.; Torruellas, W. E.; Zanoni, R. *Mat. Res. Soc. Symp. Proc.* **1991**, *247*, 151-162. (b) Guo, D.; Mazumdar, S.; Dixit, S. N. *Synth. Met.* **1992**, *49-50*, 1-11. (c) Kawabe, Y.; Jarka, F.; Peygambarian, N.; Guo, D.; Mazumdar, S.; Dixit, S. N.; Kajzar, F. *Phys. Rev. B* **1991**, *44*, 6530-6533.

(55) Burgi, H. B.; Dunitz, J. D. *J. Chem. Soc., Chem. Comm.* **1969**, 472-473.

(56) Odian, G.; Yang, N. -L.; Wei, Y. *Magnetic Reson. Chem.* **1985**, *23*, 908-915.

(57) (a) Yang, C. -J.; Jenekhe, S. A. in ref 2b, pp. 197-204. (b) Yang, C. -J.; Jenekhe, S. A.; Meth J. S; Vanherzeele, H. *Polym. Adv. Technol.* **1994**, *5*, 161-170.

(58) (a) Kanabara, H.; Kobayashi, H.; Kaino, T.; Ooba, N; Kurihara, T. *J. Phys. Chem.* **1994**, *98*, 12270-12277; (b) Geisler, T.; Petersen, J.C.; Bjornholm, T.; Fischer, E.; Larsen, J.; Dehu, C.; Brédas, J. L.; Tormos, G. V; Nugara, P. N.; Cava, M.P.; Metzger, R. M. *J. Phys. Chem.* **1994**, *98*, 10102-10111.

(59) (a) Li, H. H. *J. Phys. Chem. Ref.* Data **1976**, *5*, 329-528; (b) Grossman, C. H.; Garito, A. F. *Mol. Cryst. Liq. Cryst.* **1989**, *168*, 255-267.

(60) Mattoussi, H.; Scrinivasarao, M.; Kaatz, P. G.; Berry, G. C. *Macromolecules* **1992**, *25*, 2860-2868.

(61) Lauchlan, L.; Etemad, S.; Chung, T. C.; Heeger, A. J.; MacDiarmid, A. G. *Phys. Rev. B* **1981**, *24*, 3701-3711.

(62)) (a)Bradley, D. D. C.; Friend, R. H. *J. Mol. Electron.* **1989**, *5*, 19-24; (b) Rauscher, U.; Bässler, H.; Bradley, D. D. C.; Hennecke, M. *Phys. Rev. B* **1990**, *42*, 9830-9836. (c) Rauscher, U.; Schutz, L.; Greiner, A.; Bässler, H. *J. Phys.: Condens. Matter* **1989**, *1*, 9751-9763.

(63) Jenekhe, S. A.; Osaheni, J. A. *Science* **1994**, *265*, 765-768.

(64) Press, W. H.; Flannerg, B. D.; Teukolsky, S. A.; Vetterling, W. T. *Numeral Recipe: The Art of Scientific Computing,* Cambridge Univ. Press: New York, **1988**.

(65) (a) Marder, S. R.; Beratan, D. N.; Cheng, L.-T. *Science* **1991**, *252*, 103-106. (b) Cheng, L.-T.; Tam. W.; Stevenson, S. H.; Meredith, G. R.; Rikken, G.; Marder, S.

R. *J. Phys. Chem.* **1991**, 95, 10631-10643. (c) Marder, S. R; Perry, J.W.; Bourhill, G.; Gorman, C. B.; Tiemann, B. G.; Mansour, K. *Science* **1993**, *261*, 186-189.

(66) McCoy, R. K.; Karasz, F. E. *Chem. Mater.* **1991**, *3*, 941-947.

(67) Laermer, F.; Elsaesser, T.; Kaiser, W. *Chem. Phys. Lett.* **1988**, *148* 119-124.

(68) (a) Tarkka, R.M.; Jenekhe, S.A. *Chem. Phys. Lett.* **1996**, *260*, 533-538; (b) Tarkka, R.M.; Zhang, X.; Jenekhe, S. A. *J. Am. Chem. Soc.* **1996**, *118*, 9438-9439.

(69) Loudon, R. *The Quantum Theory of Light,* 2nd Ed., Oxford Univ. Press: New York, **1983**, pp. 26-30.

(70) Zhou, Q. L.; Shi, R. F.; Zamani-Khamari, O.; Garito, A. F. *Nonlinear Optics* **1993**, *6*, 145-154.

Table 1. The lowest-energy π-π^* optical transition (λ_{max}) and associated optical absorption edge (E_g) of conjugated polyimine thin films.

Polymer	λ_{max} (nm)	E_g (eV)
1a, PPI	405	2.50
1b, PMPI	405	2.50
2a, PPI/PMPI	405	2.50
3a, PMOPI	450	2.34
3b, PHOPI	495	2.07
3c, MO-PHOPI	510	2.03
4a, PBPI	420	2.53
4b, PSPI	430	2.38
4c, PBEPI	370	2.83

Table 2. Notation of the fitting parameters of 2-level, 3-level, and 4-level SOS theoretical models.

model	fixed parameter	optimized parameter
2-level		1. energy level of $1B_u$ state, E_{01} 2. linewidth of $1B_u$ state, S_{01} 3. transition dipole between $1A_g$ and $1B_u$ state, μ_{01}
3-level		1. energy level of $1B_u$ state, E_{01} 2. energy level of mA_g state, E_{02} 3. linewidth of $1B_u$ state, S_{01} 4. linewidth of mA_g state, S_{02} 5. transition dipole between $1A_g$ and $1B_u$ state, μ_{01} 6. transition dipole between $1B_u$ and mA_g state, μ_{12}
4-level	1. energy level of $1B_u$ state, E_{01}[a] 2. linewidth of $1B_u$ state, S_{01}[a] 3. energy level of nB_u state, E_{03}[b]	1. energy level of mA_g state, E_{02} 2. linewidth of mA_g state, S_{02} 3. linewidth of nB_u state, S_{03} 4. transition dipole between $1A_g$ and $1B_u$ state, μ_{01} 5. transition dipole between $1B_u$ and mA_g state, μ_{12} 6. transition dipole between $1A_g$ and nB_u state, μ_{03} 7. transition dipole between mA_g and nB_u state, μ_{23}

a. fixed at values obtained from the 3-level model fit.
b. by assigning the resonance peak next to the 3-photon resonance of $1B_u$ state as the 3-photon resonance of nB_u state.

Table 3. Fitting parameters of the SOS model analyses of the $|\chi^{(3)}(-3\omega;\omega,\omega,\omega)|$ spectra of conjugated polyimines.

polymer	Number density $N(10^{21}\ cm^{-3})$	E_{01}(eV) S_{01}(eV) $\mu_{(01)}$D	E_{02}(eV) S_{02}(eV) μ_{12}(D)	E_{03}(eV) S_{03}(eV) μ_{03}(eV) μ_{23}(D)
PPI[a]	3.56	2.79 0.34 16.31(10.94)[d]	3.65 0.29 8.78	3.85 0.30 7.89 -41.87
PMPI[b]	3.24	2.71 0.68 23.47(8.56)[d]	4.16 0.61 27.38	
PPI/PMPI[a]	3.40	2.80 0.34 14.59(10.68)[d]	2.01 0.36 21.89	4.00 0.15 16.47 -30.10
PMOPI[a]	2.83	2.50 0.27 25.93(10.67)[d]	2.63 0.49 16.65	4.11 0.38 7.86 -4.05
PHOPI[a]	3.37	2.26 0.20 11.69(12.17)[d]	2.79 0.13 7.80	2.97 0.39 11.95 -9.78
MO-PHOPI[a]	3.00	2.21 0.18	2.58 0.20	2.76 0.34 -28.32
PBPI[b]	2.60	20.42(10.96)[d] 2.92 0.48 27.21(11.76)[d]	16.72 2.62 0.21 7.90	13.75
PSPI[b]	2.33	2.54 0.26 8.04(8.64)[d]	2.56 0.38 24.77	
PBEPI[c]	2.54	3.01 0.58 17.60(8.99)[d]		

a. 4-level model
b. 3-level model
c. 2-level model
d. transition dipole moment obtained from the integration of the absorption spectrum.

Table 4. Off-resonant, three-photon resonance enhanced, and SOS model prediction of zero-frequency $\chi^{(3)}$.

polymer	$\lvert\chi^{(3)}\rvert$ (10^{-12}esu)		predicted (ω=0) $\chi^{(3)}$	
	three-photon resonance	off-resonance (at 2.38 μm)	model	$\chi^{(3)}$ (10^{-12}esu)
PPI	16.0	1.6	4-level	-1.55
PMPI	6.4	0.9	3-level	-0.43
PPI/PMPI	19.0	2.3	4-level	-1.99
PMOPI	52.0	7.3	4-level	-4.61
PHOPI	11.0	2.3	4-level	-1.63
MO-PHOPI	72.0	16.3	4-level	-8.12
PBPI	32.0	5.2	3-level	-5.70
PSPI	9.5	1.1	3-level	0.42
PBEPI	4.5	1.0	2-level	-0.90

Figure Captions

Chart 1. Molecular structures of conjugated aromatic polyimines.

Chart 2. Schematic representation of 2-level, 3-level, and 4-level SOS models.

Chart 3. Schematic representation of the molecular exciton states in the optical response of conjugated polyimines.

Figure 1. Optical absorption spectra of (a)PPI, (b) PBPI, (c) PSPI, and (d) PBEPI thin films.

Figure 2. Optical absorption spectra of (a) PPI, (b) PMOPI, (c) PHOPI, and (d) MO-PHOPI thin films.

Figure 3. Optical absorption spectra of (a) PPI, (b) PMPI, and (c) PPI/PMPI thin films.

Figure 4. The optical transmission spectrum and refractive-index dispersion of PMPI. The solid line is the three-term Sellmeir equation fit of the refractive index data.

Figure 5. Fluorescence spectra of PMOPI excited at various wavelengths.

Figure 6. Fluorescence energy (at emission λ_{max}) of PMOPI as a function of excitation light energy.

Figure 7. Two-level (dot), three-level(dash), and four-level(solid line) model fits of the $|\chi^{(3)}(-3\omega;\omega,\omega,\omega)|$ dispersion data of PPI.

Figure 8. $|\chi^{(3)}(-3\omega;\omega,\omega,\omega)|$ dispersion data for (a) PPI, (b) PBPI, (c) PSPI, and (d) PBEPI. Solid lines are the theoretical models: four-level (PPI), three-level (PBPI and PSPI), and two-level (PBEPI).

Figure 9. $|\chi^{(3)}(-3\omega;\omega,\omega,\omega)|$ dispersion data for (a) PPI, (b) PMOPI, (c) PHOPI, and (d) MO-PHOPI. Solid lines are the theoretical models: four-level (PPI, PMOPI, MO-PHOPI) and three-level (PHOPI).

Figure 10. $|\chi^{(3)}(-3\omega;\omega,\omega,\omega)|$ dispersion data for (a) PPI, (b) PMPI, and (c) PPI/PMPI. Solid lines are the theoretical models: four-level (PPI and PPI/PMPI) and three-level (PMPI).

Figure 11. Four-level model prediction of the real (dot) and imaginary (dash) components of $\chi^{(3)}(-3\omega;\omega,\omega,\omega)$ for PPI.

Figure 12. Four-level model prediction of the magnitude (solid line), real (dot), and imaginary (dash) components of $\chi^{(3)}(-\omega;\omega,-\omega,\omega)$ for MO-PHOPI.

Chart 1

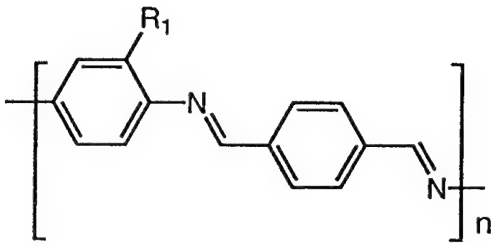

1a, R_1= H (PPI)
1b, R_1= CH_3 (PMPI)

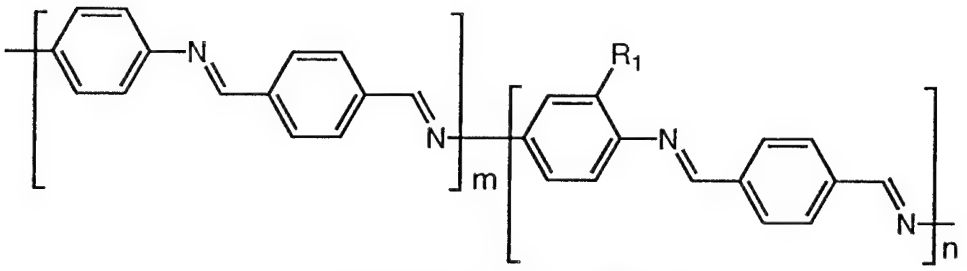

2a, R_1= CH_3 (PPI/PMPI)

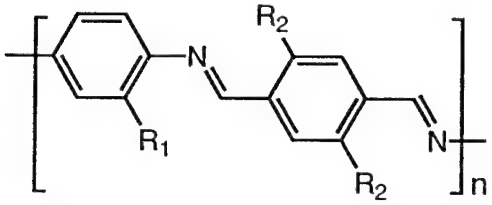

3a, R_1= H, R_2= OCH_3 (PMOPI)
3b, R_1= H, R_2= OH (PHOPI)
3c, R_1= OCH_3, R_2= OH (MO-PHOPI)

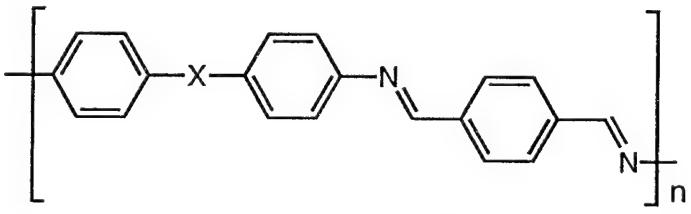

4a, X= —— (PBPI)

4b, X= 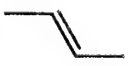 (PSPI)

4c, X= —O— (PBEPI)

Chart 2

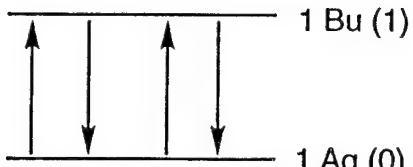

(a)

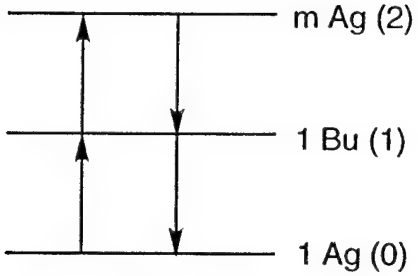

(b)

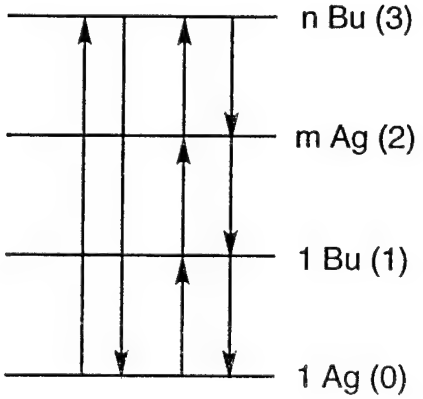

(c)

Chart 3

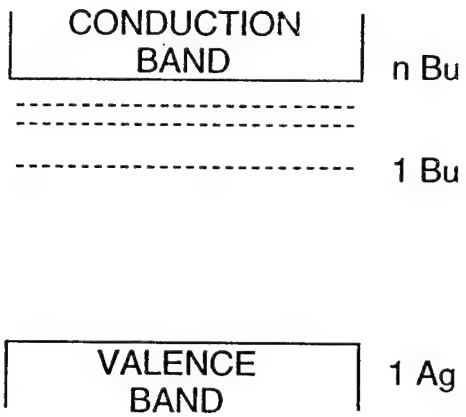

Scheme 1

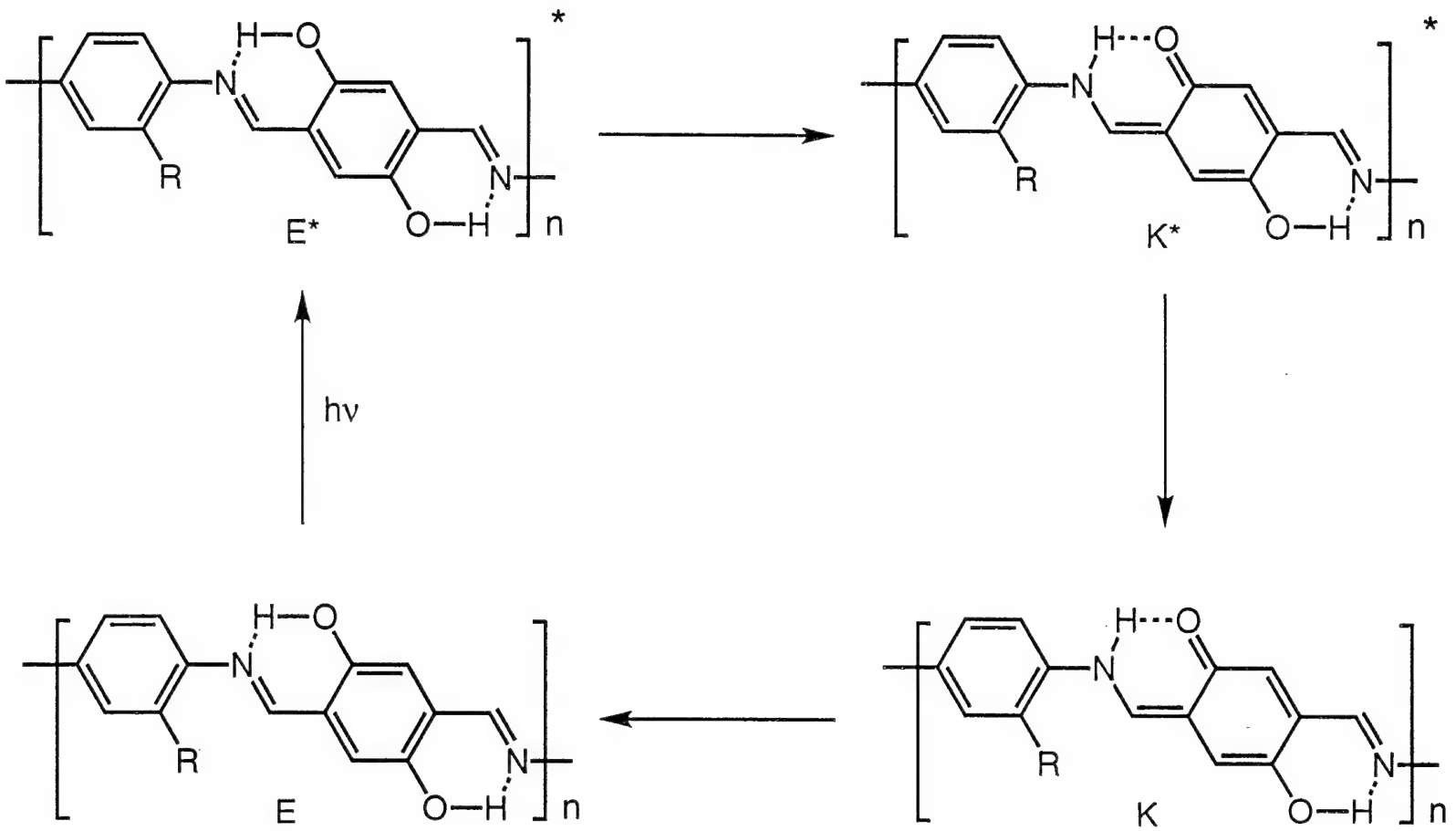

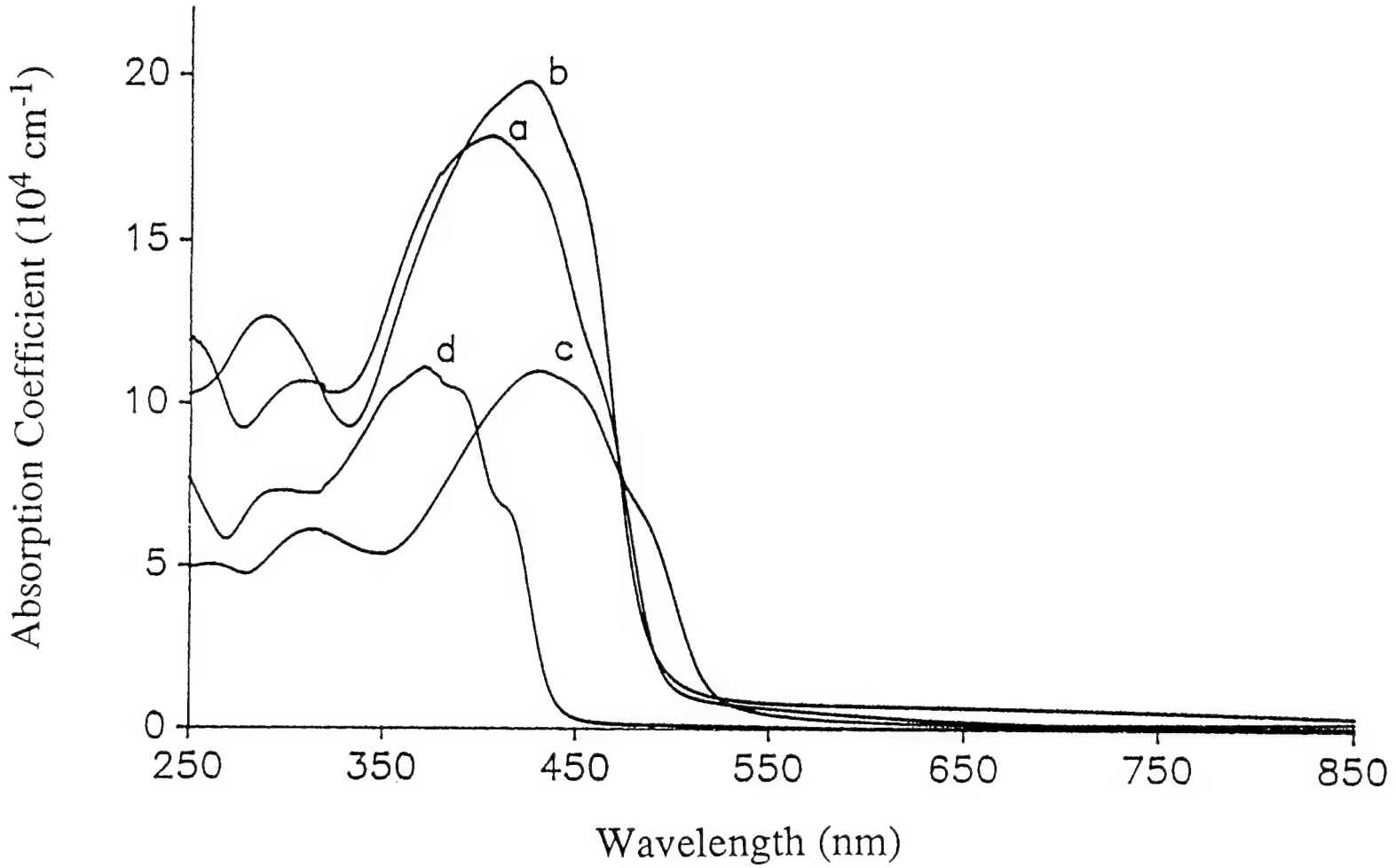
Absorption Coefficient (10^4 cm^{-1})
20
15
10
5
0
250
350
450
550
650
750
850
Wavelength (nm)
a
b
c
d

Fig. 1

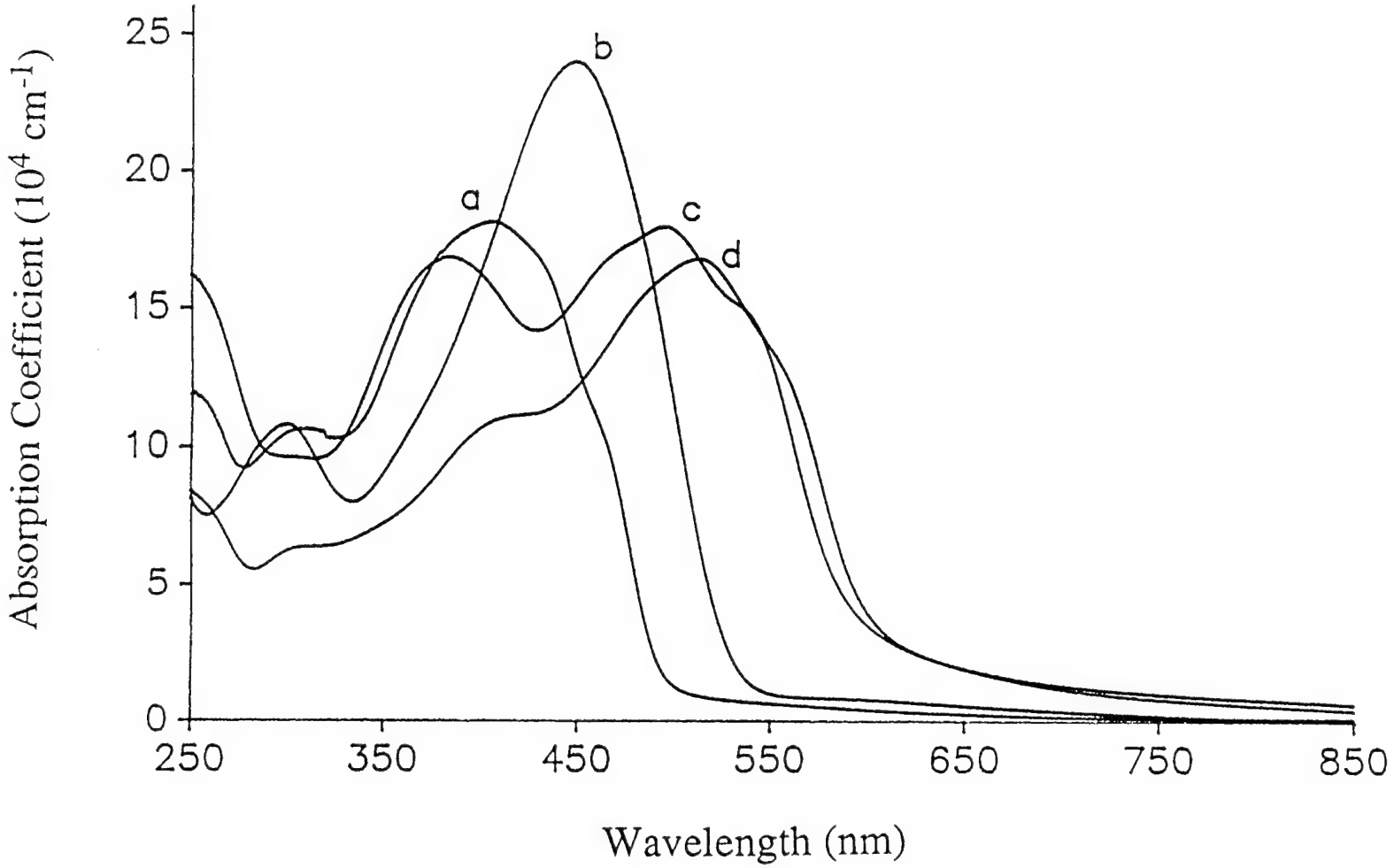
Absorption Coefficient (10^4 cm^{-1})
25
20
15
10
5
0
250
350
450
550
650
750
850
Wavelength (nm)
a
b
c
d

7. Fig. 4

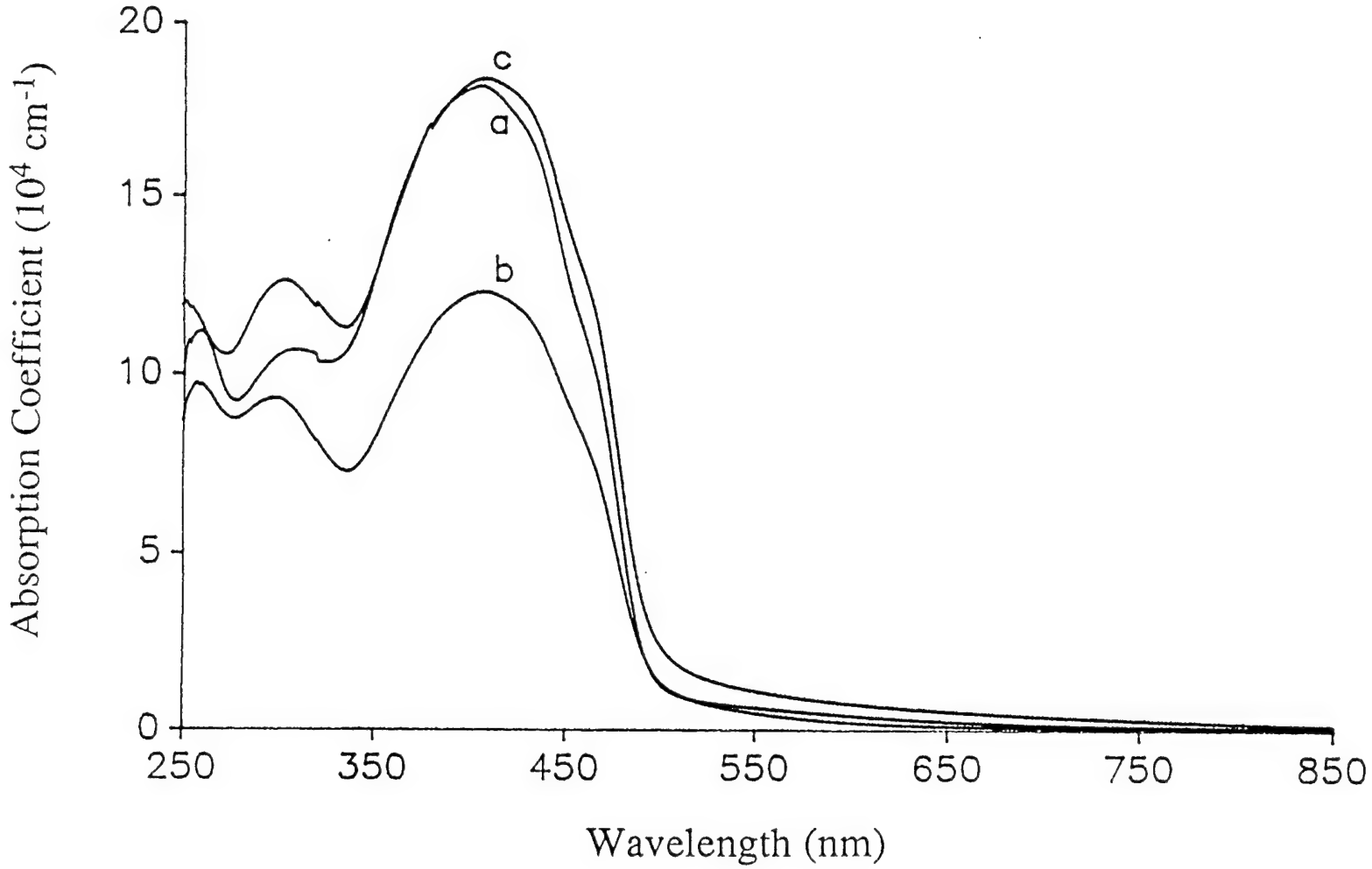
Absorption Coefficient (10^4 cm^{-1})
20
15
10
5
0
250
350
450
550
650
750
850
Wavelength (nm)
a
b
c

Fig. 5

Fig. 4

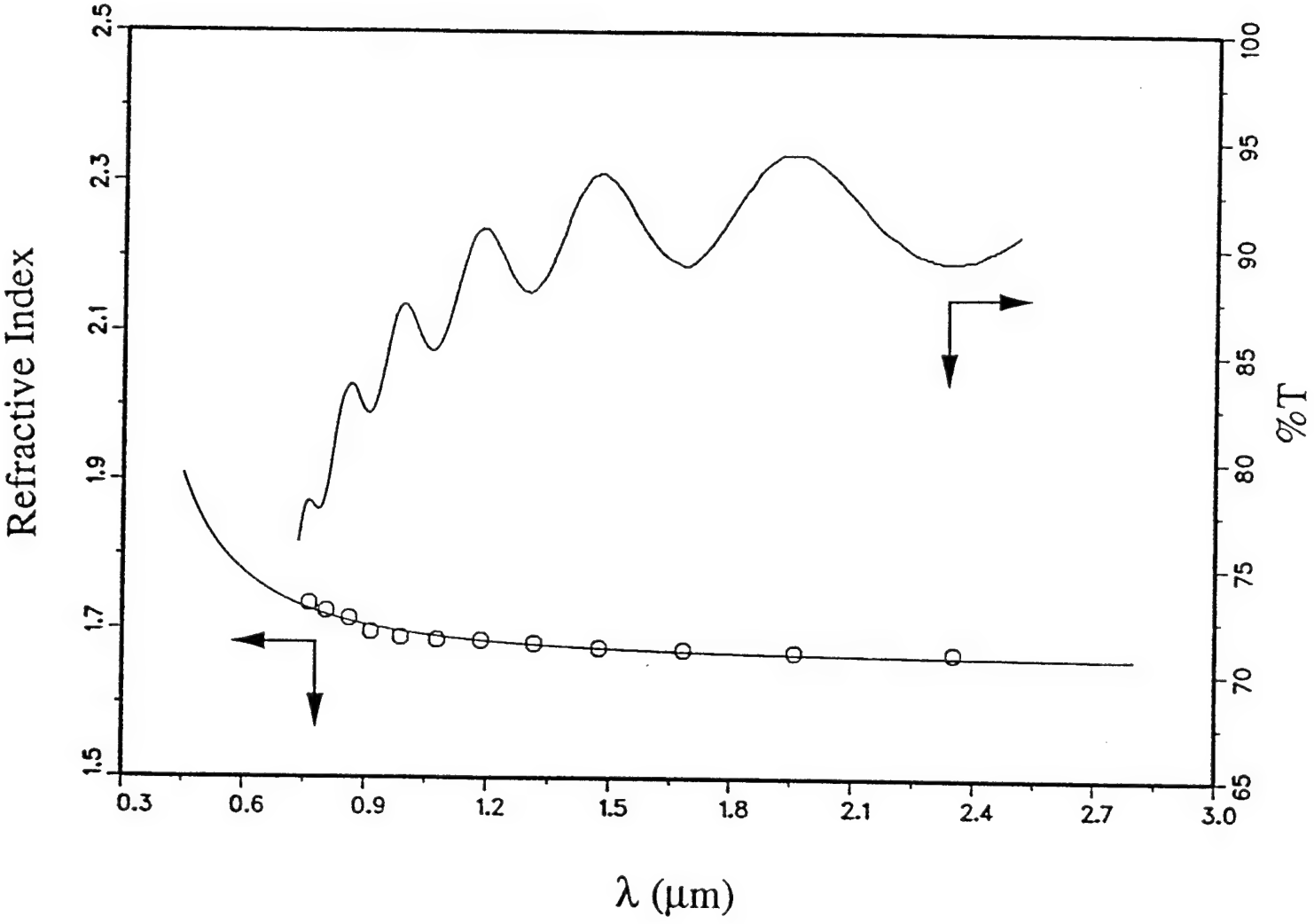
Refractive Index
2.5
2.3
2.1
1.9
1.7
1.5
%T
100
95
90
85
80
75
70
65
0.3
0.6
0.9
1.2
1.5
1.8
2.1
2.4
2.7
3.0
λ (μm)

Fig. 5

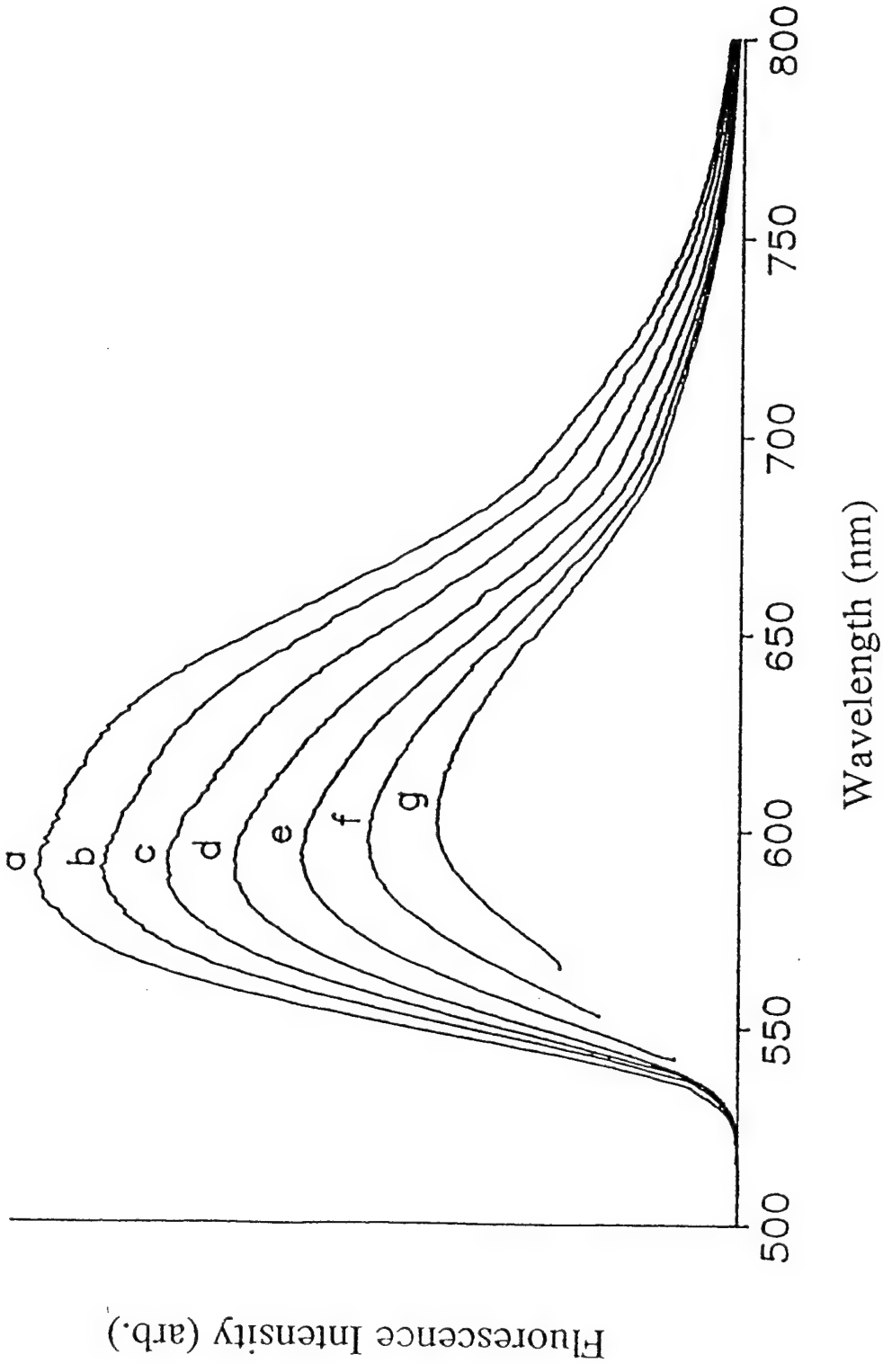
Fluorescence Intensity (arb.)
500
550
600
650
700
750
800
Wavelength (nm)
a
b
c
d
e
f
g

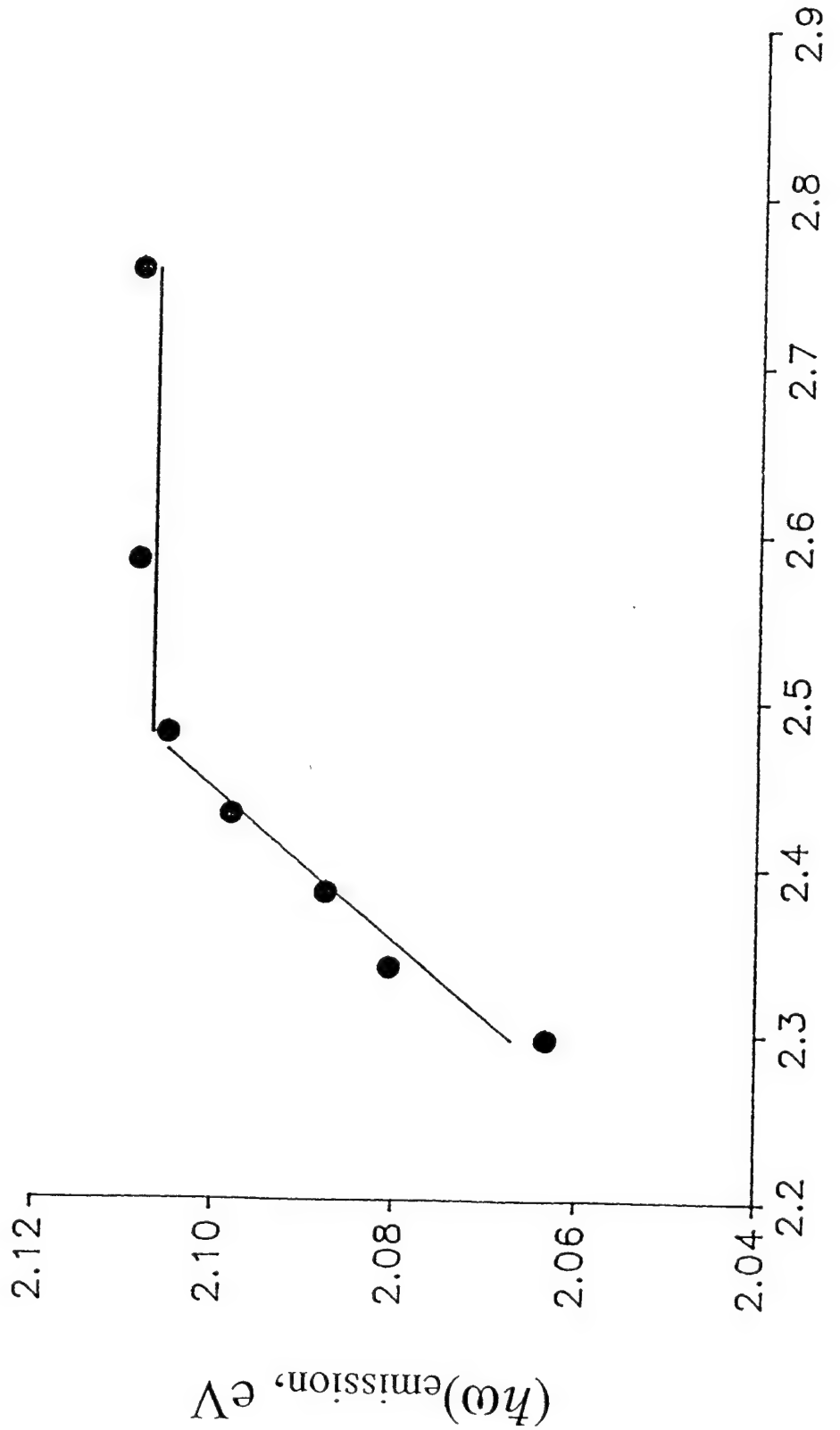
2.12
2.10
2.08
2.06
2.04
2.2
2.3
2.4
2.5
2.6
2.7
2.8
2.9
$(\hbar\omega)_{emission}$, eV
$(\hbar\omega)_{excitation}$, eV

Fig. 6

Fig. 7

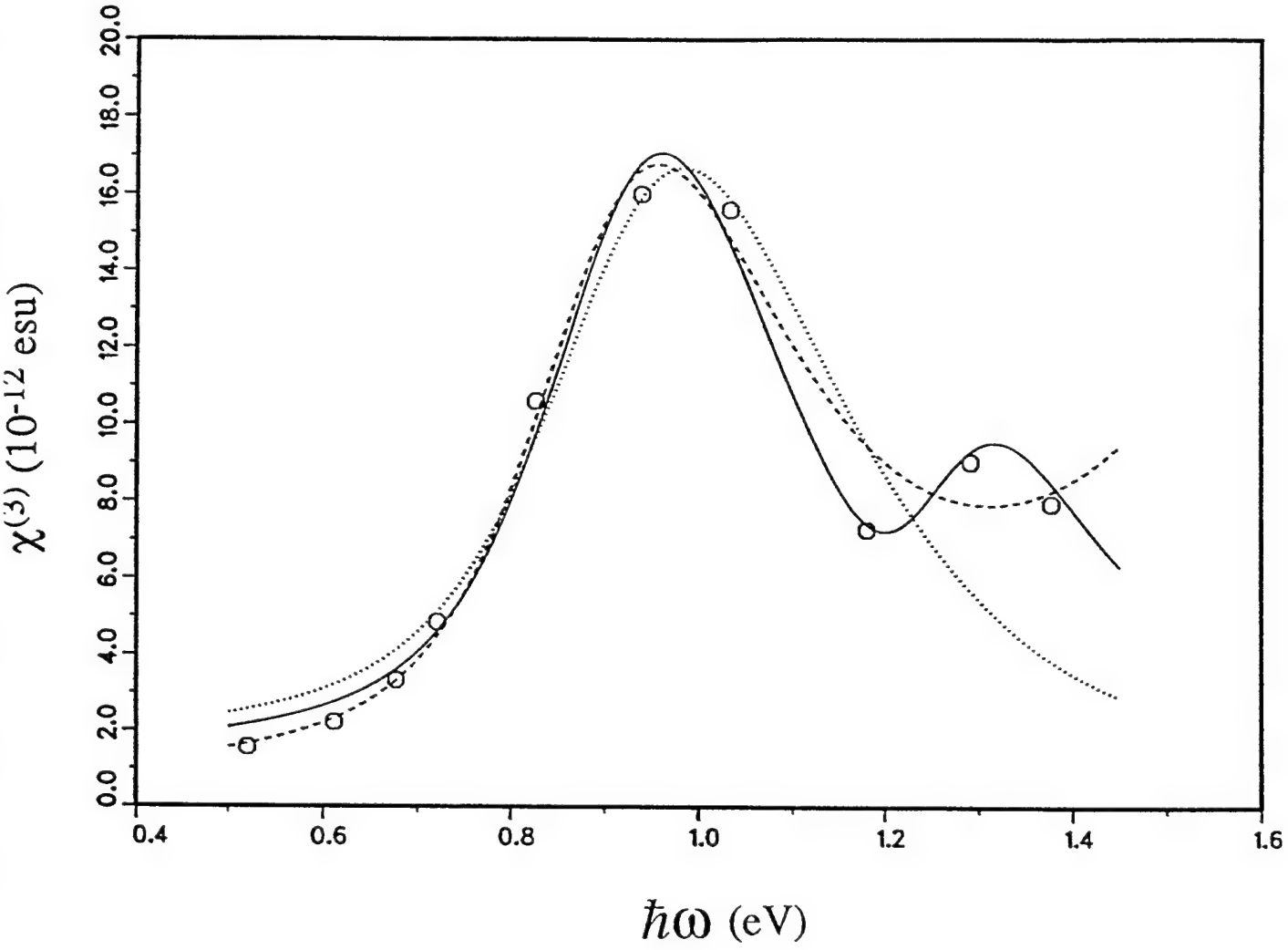
$\chi^{(3)}$ (10^{-12} esu)
0.0
2.0
4.0
6.0
8.0
10.0
12.0
14.0
16.0
18.0
20.0
0.4
0.6
0.8
1.0
1.2
1.4
1.6
$\hbar\omega$ (eV)

Fig. 8

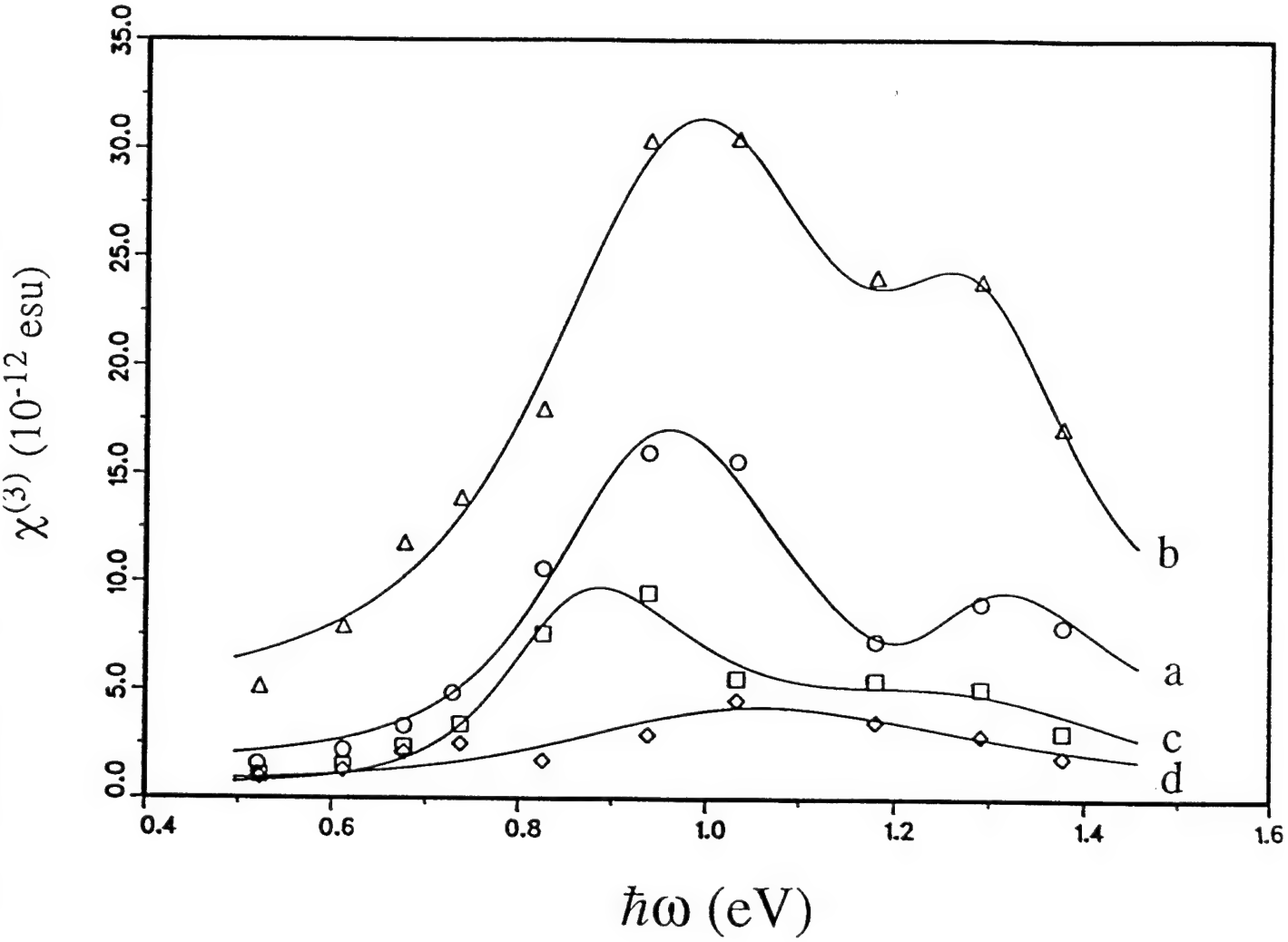
$\chi^{(3)}$ (10^{-12} esu)
35.0
30.0
25.0
20.0
15.0
10.0
5.0
0.0
0.4
0.6
0.8
1.0
1.2
1.4
1.6
$\hbar\omega$ (eV)
b
a
c
d

Fig. 9

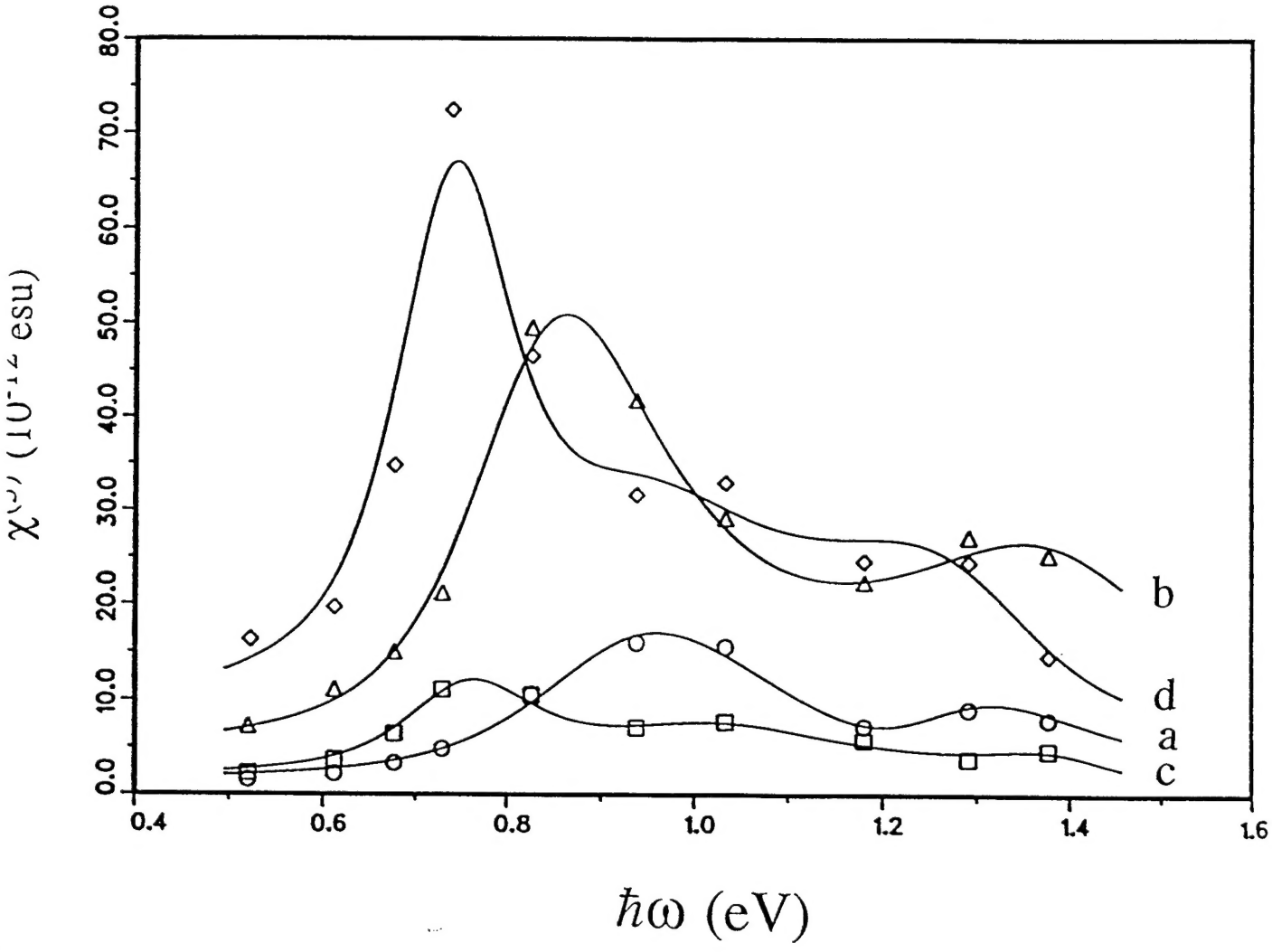

Fig. 10

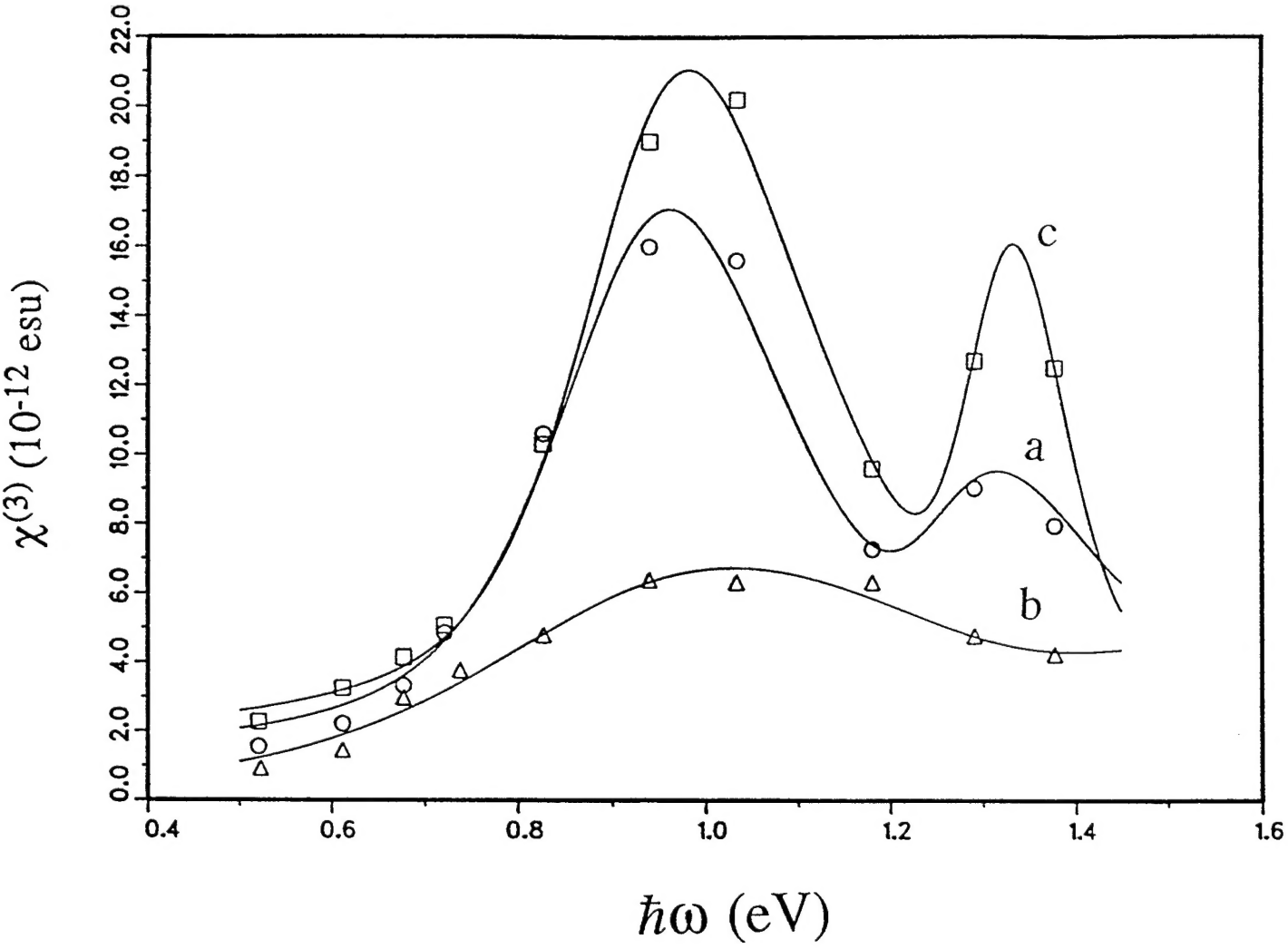
$\chi^{(3)}$ (10^{-12} esu)
0.0
2.0
4.0
6.0
8.0
10.0
12.0
14.0
16.0
18.0
20.0
22.0
0.4
0.6
0.8
1.0
1.2
1.4
1.6
$\hbar\omega$ (eV)
a
b
c

Fig. 11

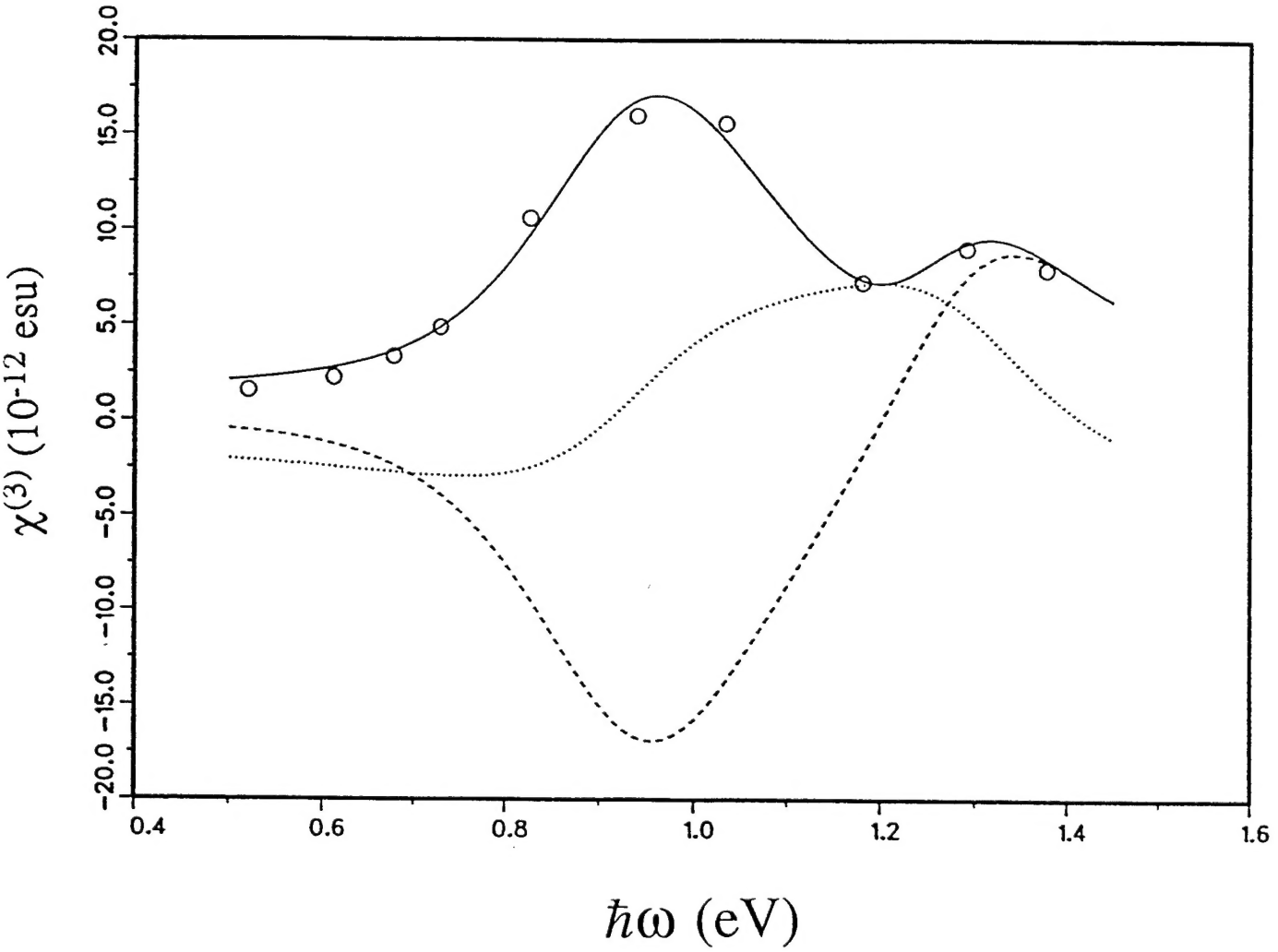
$\chi^{(3)}$ (10^{-12} esu)
20.0
15.0
10.0
5.0
0.0
-5.0
-10.0
-15.0
-20.0
0.4
0.6
0.8
1.0
1.2
1.4
1.6
$\hbar\omega$ (eV)

Fig. 12

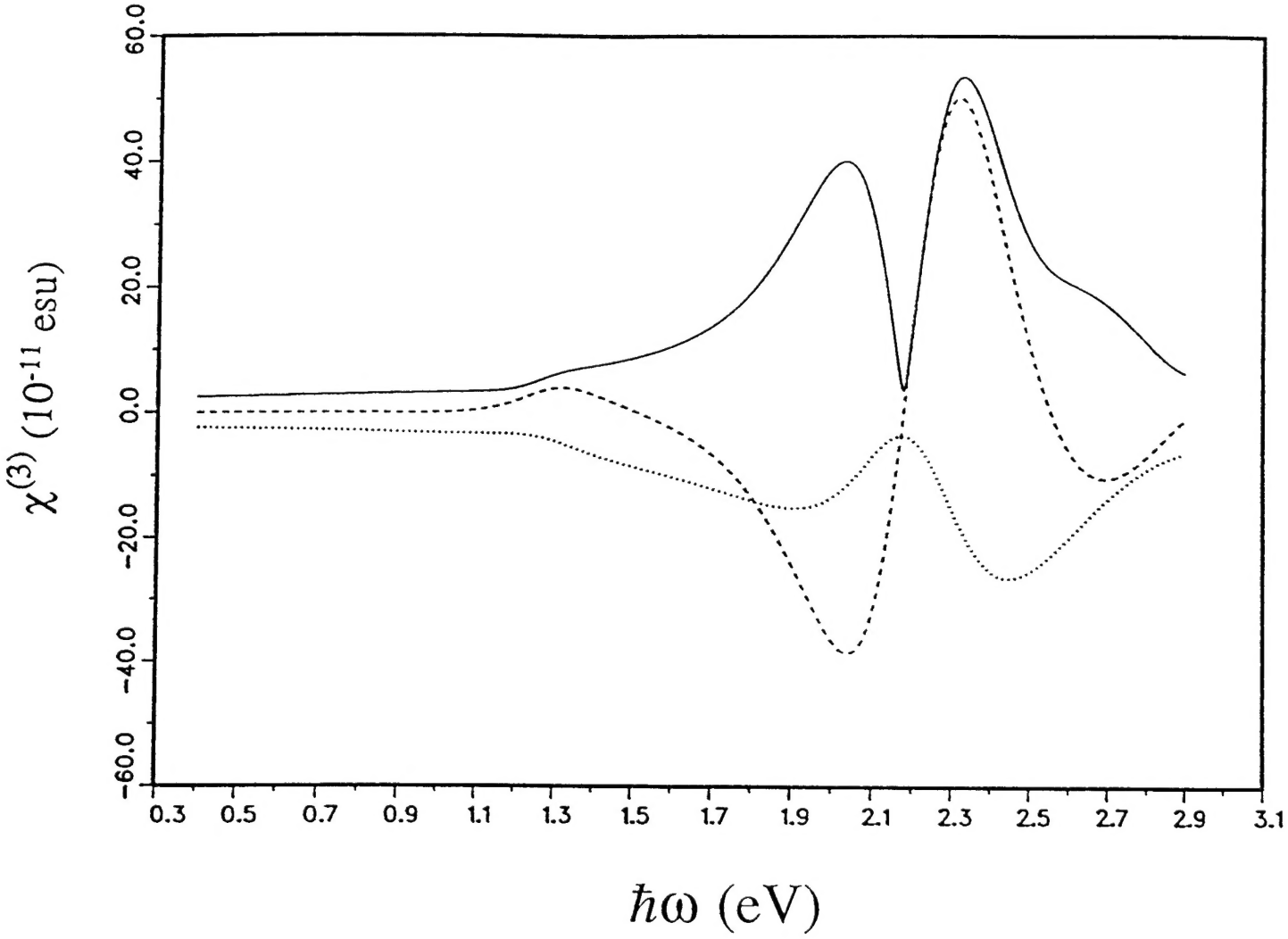
60.0
40.0
20.0
0.0
-20.0
-40.0
-60.0
0.3
0.5
0.7
0.9
1.1
1.3
1.5
1.7
1.9
2.1
2.3
2.5
2.7
2.9
3.1
$\chi^{(3)}$ (10^{-11} esu)
$\hbar\omega$ (eV)